

REPORT DOCUMENTATION PAGE

Form Approved

OMB No. 0704-0188

Public reporting burden for this collection of information is estimated to average 1 hour per response, including the time for reviewing instructions, searching existing data sources, gathering and maintaining the data needed, and completing and reviewing the collection of information. Send comments regarding this burden estimate or any other aspect of this collection of information, including suggestions for reducing this burden, to Washington Headquarters Services, Directorate for Information Operations and Reports, 1215 Jefferson Davis Highway, Suite 1204, Arlington, VA 22202-4302, and to the Office of Management and Budget, Paperwork Reduction Project (0704-0188), Washington, DC 20503.

1. AGENCY USE ONLY (Leave blank)		2. REPORT DATE January 17 1997		3. REPORT TYPE AND DATES COVERED FINAL REPORT 20 Oct 93 - 19 Oct 96	
4. TITLE AND SUBTITLE Luminescence and Electroluminescence Properties of Rare Earth Doped GaAs, InP and GaN				5. FUNDING NUMBERS 61102F 2305/FS AFOSR-TR-97-0070	
6. AUTHOR(S) Principal Investigator: Professor DSc. Dr. H. J. Lozykowski					
7. PERFORMING ORGANIZATION NAME(S) AND ADDRESS(ES) Ohio University Office of Research and Sponsored Programs Athens, Ohio 45701-2979					
9. SPONSORING/MONITORING AGENCY NAME(S) AND ADDRESS(ES) AFOSR / NE Building 410 Bolling AFB, DC 20332-6448				10. SPONSORING/MONITORING AGENCY REPORT NUMBER F49620-94-1-0024	
11. SUPPLEMENTARY NOTES 19970131 059					
12a. DISTRIBUTION/AVAILABILITY STATEMENT APPROVED FOR PUBLIC RELEASE: DISTRIBUTION UNLIMITED				12b. DISTRIBUTION CODE	
13. ABSTRACT (Maximum 200 words) This research report contains progress in studies of the photoluminescence, and cathodoluminescence of the rare earth doped wide bandgap semiconductors. Photoluminescence and cathodoluminescence of GaN layer grown by MOCVD on (0001) sapphire substrate, undoped and n-type Si doped from Cree, and EMCORE. Temperature dependence of the near bandgap emission and donor acceptor pairs were investigated under excitation by He-Cd laser (325nm), and an electron beam (5 KeV). The photoluminescence and cathodoluminescence spectra show a similar feature. For all sample the PL lines we found a continuous decrease of the peak energy with increasing temperature following the shift of the bandgap. Photoluminescence of GaN implanted with phosphorus(200KeV) shows the broad luminescence bands near 2.98 eV and 2.88 eV, and must be associated with the presence of these impurities in the system. The energies indicate impurity levels about 0.52eV and 0.62 eV from the band edges. We also synthesis and growth of single crystals of GaN (needle single crystals ~ 4 mm long and 10- 30 µm in diameter was growth). The preliminary results of PL, CL and kinetics of ZnO doped with Dy, Er, Tm, and co-doped with Li, are promising, we obtained for the first time ever strong rare earth PL and CL emission at room temperature. The photoluminescence study of microcrystalline powders of GaN doped with Dy, Er, Tm, Nd, codoped with Li, and GaN implanted with Er, Tm, Nd, and co-implanted with oxygen are in progress. The PL kinetics of p-type GaAs Nd implanted and MOCVD grown crystals were studied under pulsed excitations. The study shows that the PL rise time depends on excitation intensity. It reflects an indirect excitation process of Nd ions. The developed theoretical model of energy transfer from the host lattice to the localized core excited states of RE isoelectronic structured traps explained experimental results.					
14. SUBJECT TERMS Luminescence and Electroluminescence Properties of Rare Earth Doped GaAs, InP and GaN				15. NUMBER OF PAGES	
				16. PRICE CODE	
17. SECURITY CLASSIFICATION OF REPORT	18. SECURITY CLASSIFICATION OF THIS PAGE	19. SECURITY CLASSIFICATION OF ABSTRACT	20. LIMITATION OF ABSTRACT		

Luminescence and Electroluminescence Properties of Rare Earth Doped GaAs, InP and GaN

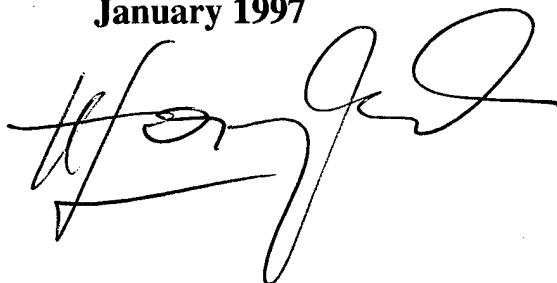
Annual Report Submitted to :

The Air Force Office of Scientific Research

by :

**Henryk J. Lozykowski
School of Electrical Engineering and Computer Science
Stocker Center,
Ohio University
Athens, Ohio 45701-2979**

January 1997

A handwritten signature in black ink, appearing to read 'H. Lozykowski', is written over the printed name and affiliation.

PERSONNEL

Faculty

H. J. Lozykowski, Professor, *Principal Investigator*

Graduate Students

A. K. Alshawa, *Ph.D. Student* (Ph.D. under final preparation, defense Winter Quarter 1997, *Partially supported by AFOSR grant*).

U. Saha, *MS. Student* , (*Partially supported by AFOSR grant*),

X.Li, *Visiting Scholar from China* (*October 1995-May 1996*)

B. H. Patel, *MS. Student*

Kanyu Cao, *MS. Student*

M. Maldei, *MS. Student*

COLLABORATORS:

Dr. I. Brown, Lawrence Berkeley Laboratory, University of California at Berkeley
(Ion Implantation, SIMS and RBS Analysis)

Dr. D.B. Poker, Oak Ridge National Laboratory, Solid State Div. Martin Marietta Energy Sys.
P.O.Box 2008, Mail Stop 6048, 1 Bethel Valley Rd. 37831
(Ion Implantation, SIMS and RBS Analysis)

M. Asif Khan, APA Optics Inc., Blaine, Minnesota
(GaN, AlGaIn, and AlN Sample Growth by SALE - MOCVD)

Scientific Papers

The following scientific papers have been published, or in preparation:

1. **U. Saha, and H. J. Lozykowski,**
"Photoluminescence Kinetics Model of P-type GaAs: Nd", Mat. Res. Soc. Symp. Proc. Vol. 422, 285, (1996).
2. **H.J. Lozykowski, A. K. Alshawa, and I. Brown,**
"Luminescence Properties of Ytterbium and Oxygen Coimplanted InP", Mat. Res. Soc. Symp. Proc. Vol. 417, 363, (1996).
3. **Tiesheng Li, H. J. Lozykowski, and J. L. Reno,**
"Photoluminescence and Photo-Current Study of a CdTe / CdZnTe Strained Layer Coupled Double Quantum Well Structure," Semiconductor Heteroepitaxy Growth, Characterization and Device Applications, editors: B. Gil and R.L. Aulombard, World Scientific,- Singapore, New Jersey, London, HongKong, 1996, pages 105-109.
4. **H.J. Lozykowski, B. H. Patel, Kanyu Cao, and M. Maldei**
"Photoluminescence Properties of ZnO, Doped with Dy, Er, Tm, Nd. Research in progres,

Presentations:

1. **H.J. Lozykowski, A. K. Alshawa, H. and I. Brown,**
"Luminescence Properties of Ytterbium and Oxygen Coimplanted InP", MRS Materials Research Society Meeting, Boston, 1995.
2. **U. Saha, and H. J. Lozykowski,**
"Photoluminescence Kinetics Model of P-type GaAs: Nd", MRS Materials Research Society Meeting, San Francisco, CA, Spring 1996.

Students:

MS Supervisions completed:

Uttam Saha,

thesis title: "Photoluminescence and Kinetics of MOCVD grown P-type GaAs: Nd, and Nd-Implanted Semi-Insulating GaAs," Spring 1996.

Michael Maldei,

thesis title: "Quantum Efficiency Measurements of A-C:H Based Photovoltaic Cells," Fall 1996.

Former

Post-Doctoral Student:

Tiesheng Li, Ph.D.,

Post-Doctor (holding Ohio University Post-Doctorate Fellowship from September 1994, till July 1995, *Partially supported by AFOSR grant* July-September 1995).

A. PhD students:

A. K. Alshawa,

dissertation title "Luminescence Properties of Rare Earth Doped III-V and II-VI Semiconductors," under final preparation, defense Winter Quarter 1997, *(In 1996 Partially supported by AFOSR grant)*.

B. PhD in progress:

Wojciech Jadwisieniczak

Tentative dissertation title "Luminescence Properties of Rare Earth and Conventional Impurities Doped GaN Semiconductor," (1998).

MS thesis in progress:

Bhavnes H. Patel,

Tentative thesis title: "Photoluminescence and Kinetics of ZnO: Dy, Li," expected defense 1997.

Kanyu Cao,

Tentative thesis title: "Photoluminescence and Cathodoluminescence of ZnO Single Crystals and sintered powders doped with Er, Nd, Tm, Ho, Pr, and Li," expected defense 1997.

Table of Contents

	Page
I Introduction	2
II Photoluminescence and Cathodoluminescence of GaN Layer Grown by MOCVD on (0001) Sapphire Substrate, Sample Preparation and Results.....	2
Table I.....	3
A. Ion Implantation	3
Table II.....	5
B. Annealing	5
Table III.....	6
C. Preliminary Results.....	6
IV Preparation of Polycrystalline GaN, and ZnO Phosphors Doped with Rare Erth and Others Impurities.....	14
Table IV.....	28
Table V.....	29
V Appendix A: Reprints of Publications 1996.....	31
1. U. Saha, and H. J. Lozykowski, "Photoluminescence Kinetics Model of P-type GaAs: Nd."	31
2. H.J. Lozykowski, A. K. Alshawa, and I. Brown, "Luminescence Properties of Ytterbium and Oxygen Coimplanted InP.".....	39
3. Tiesheng Li, H. J. Lozykowski, and J. L. Reno, "Photoluminescence and Photo-Current Study of a CdTe / CdZnTe Strained Layer Coupled".....	48

I INTRODUCTION

This research report contains progress in studies of the photoluminescence, and cathodoluminescence of the rare earth doped widebandgap semiconductors.

- a. Photoluminescence and cathodoluminescence of GaN layer grown by MOCVD on (0001) sapphire substrate, undoped and n-type Si doped.
- b. * Synthesis and growth of single crystals of gallium nitride.
** Synthesis microcrystalline powders of GaN: doped with Dy, Er, Tm, Nd, Tb, and codoped with O, Li, Na, and F.
- c. GaN: implanted with Er, Tm, Nd, and coimplanted with oxygen.
- d. GaN: implanted with P (phosphorus).
- e. Photoluminescence of ZnO single crystals doped with Er, Nd, Pr, and Ho by implantation.
- f. Microcrystalline powder and sintered pellets of ZnO doped with Dy, Nd, Tm, Er, codoped with lithium and without lithium.

II Photoluminescence and Cathodoluminescence of GaN Layer Grown by MOCVD on (0001) Sapphire Substrate, Sample Preparation and Results.

Table I

Type of samples	Concentration[cm ⁻³]	Source
n-type GaN	2×10 ¹⁶	#5 CREE
n-type GaN	5×10 ¹⁵	#8 CREE
GaN doped Si	6×10 ¹⁷	#7 CREE
GaN	5×10 ¹⁶	#6 CREE
n-type GaN	2×10 ¹⁷	#11 EMCORE
GaN doped Si		#10 EMCORE
p-type GaN		#9 EMCORE
GaN		#1 APA OPTICS
GaN		#2 APA OPTICS

A. Ion Implantation

The ion implantation of rare earth was done by Dr. I. G. Brown from Lawrence Berkeley Laboratory at the University of California, Berkeley. Implantation of Nd^{3+} , Yb^{3+} , and Tm^{3+} were performed with an unconventional implantation technique using a new kind of high current metal ion source developed at Berkeley. The maximum implantation energy is 160 KeV. The co-implantation of oxygen was done at IICO Corp, Santa Clara, California. For the oxygen co-implantation, the dosage and implantation energy was chosen to overlap profiles of rare earth as seen in Fig 1. The implantation conditions are shown in Tables II and III. Samples do not show rare earth photoluminescence emission after implantation and annealing at 700 °C. No erbium luminescence was detected. Recently, the above samples were co-implanted with oxygen at energy 35 keV and dose $1 \times 10^{15} \text{ cm}^{-2}$ to enhance the luminescence of rare earth. The implantation of oxygen was done by IICO Corporation, Santa Clara California. The investigations of optical properties of GaN doped with rare earth are currently in progress. The annealing process after implantation in N_2 or forming gas may degrade the implanted region and be responsible for absence of rare earth luminescence. To protect the implanted GaN surface from degradation during annealing, we will deposit thin layers of GaN, or other materials like Al_2O_3 , ErF , Ga_2O_3 . The construction of the electron beam evaporation system is in final stage. We also are investigating GaN thin film's monocrystals purchased from Cree Industries, and EMCORE implanted with Er^{3+} at high energy (1 MeV), and coimplanted with oxygen (98 KeV) (Table II). The investigations of GaN implanted with Nd^{3+} , and Tm^{3+} , at energy 1-2 MeV, are postponed to the near future because Dr. Poker from Oak Ridge National Laboratory, experienced some difficulties with the implanter. The implanted crystals will be analyzed by SIMS and RBS technics. The luminescence property will be investigated using photo excitation and electron beam excitations with energy from 100 eV-5KeV.

Figure 1

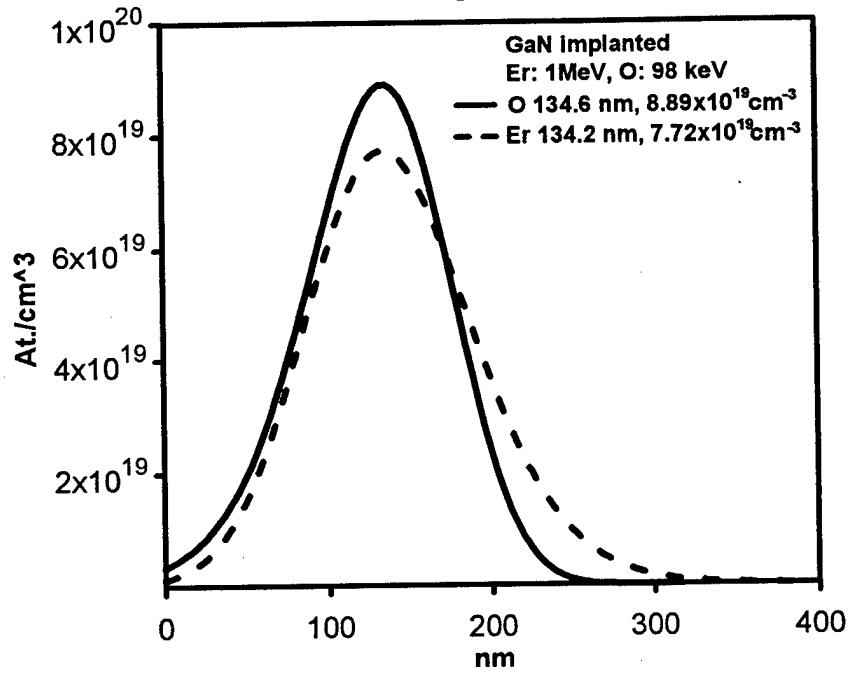


Figure 2

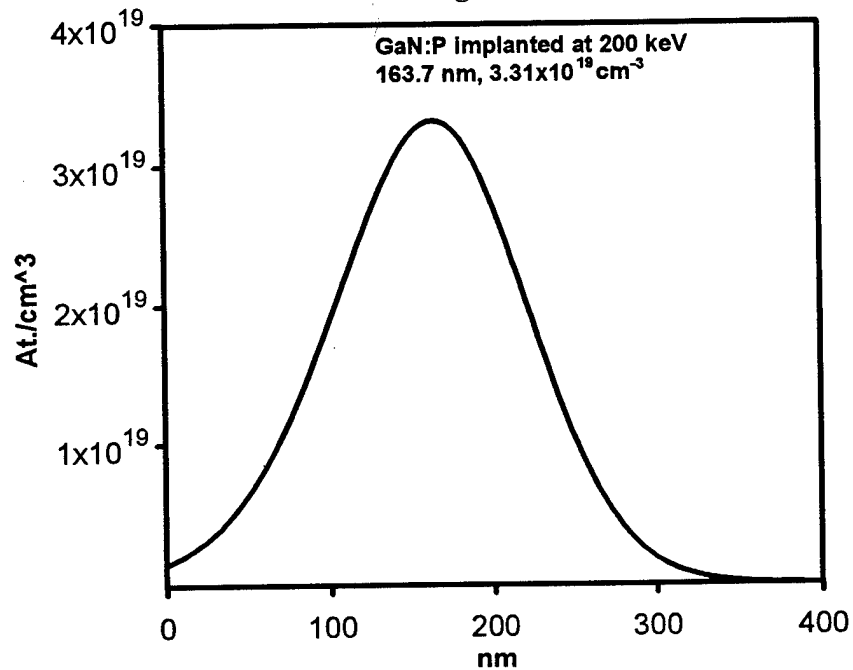


Fig.1 Depth distribution of Er ions implanted in GaN at 1 MeV and co-implanted with oxygen at 98 KeV, calculated using Ion beam profile code V-3.20 software. Fig.2 show distribution of phosphorus implanted at 200 KeV.

Table II

Samples	Implantation fluence and energy of rare earth and oxygen	Annaling condition
GaN:Er,O	$1 \times 10^{15} \text{ cm}^{-2}$, 1 MeV, 98 keV	1hr at 1000°C , in NH_3
GaN:Er,O	$1 \times 10^{15} \text{ cm}^{-2}$, 1 MeV, 98 keV	0.5hr at 900°C , in NH_3
GaN:Er,O	$1 \times 10^{15} \text{ cm}^{-2}$, 1 MeV, 98 keV	20 sec at 700°C , in N_2
GaN:Er,O	$1 \times 10^{14} \text{ cm}^{-2}$, 165 keV, 35 keV	20 sec at 750°C , in N_2
GaN:Er,O	$1 \times 10^{14} \text{ cm}^{-2}$, 165 keV, 35 keV	20 sec at 800°C , in N_2
GaN:Er,O	$1 \times 10^{14} \text{ cm}^{-2}$, 165 keV, 35 keV	20 sec at 900°C , in N_2
GaN:Er,O	$1 \times 10^{14} \text{ cm}^{-2}$, 165 keV, 35 keV	20 sec at 970°C , in N_2
GaN:Er:Yb,O	$1 \times 10^{14} \text{ cm}^{-2}$, 165 keV, 35 keV	20 sec at 750°C , in N_2
AlGaN:Er,O	$1 \times 10^{14} \text{ cm}^{-2}$, 165 keV, 35 keV	

B. Annealing

Because implanted ions can occupy different types of sites (e.g., interstitial or substitutional) in GaN, the optical activity of the implanted ions can be strongly dependent on the annealing temperature of the implanted samples.

The GaN samples were cut to small pieces ($4 \times 4 \text{ mm}^2$) and then cleaned by standard methods. The annealing process was performed using two methods, the first utilized the rapid thermal annealing apparatus designed and built in our laboratory for annealing at different temperatures up to 1000°C for 10 sec and to a maximum of 25 minutes. The annealing process was performed in ambient of N_2 , or a forming gas in graphite circular box 3 mm high. The samples are placed, implanted face down, on GaN crystal in a graphite box is covered with a graphite lid of 1 mm thickness and placed on the tantalum strip heater. The sample implanted face down on GaN crystal to maintained stoichiometry of an annealed sample. The temperature is measured by a microprocessor controlled temperature indicator OMEGA model 650 through a thermocouple placed inside the bottom of the graphite box. The rise

time of the temperature was controlled by the AC voltage applied to the strip heater. For temperatures up to 900 °C, our system maintains a rise time of 6 second and a decay time from 900 °C to 500 °C of 22 seconds. The second method we used was the close proximity cap method, annealed samples of GaN face to face were placed in a tube furnace at different temperature and duration of time in ammonia or N₂ ambient. The photoluminescence investigation of the Er, Nd, and Tm doped GaN thin films' crystals are in progress. We observed only weak PL emission at 1540 nm from erbium and oxygen implanted and annealed GaN samples.

Table III

Samples	Annaling Condition
GaN:P ($5 \times 10^{14} \text{ cm}^{-2}$, 200KeV)	1 hrs at 400 ⁰ C, in NH ₃
GaN:P ($5 \times 10^{14} \text{ cm}^{-2}$, 200KeV)	1 hrs at 500 ⁰ C, in NH ₃
GaN:P ($5 \times 10^{14} \text{ cm}^{-2}$, 200KeV)	1 hrs at 600 ⁰ C, in NH ₃
GaN:P ($5 \times 10^{14} \text{ cm}^{-2}$, 200KeV)	1 hrs at 700 ⁰ C, in NH ₃
GaN:P ($5 \times 10^{14} \text{ cm}^{-2}$, 200KeV)	1 hrs at 900 ⁰ C, in NH ₃
GaN:P ($5 \times 10^{14} \text{ cm}^{-2}$, 200KeV)	1 hrs at 1000 ⁰ C, in NH ₃
GaN:P ($5 \times 10^{14} \text{ cm}^{-2}$, 200KeV)	1 hrs at 1100 ⁰ C, in NH ₃
Samples	Rapid Thermal Annaling
GaN:P ($5 \times 10^{14} \text{ cm}^{-2}$, 200KeV)	15 sec at 850 ⁰ C, in N ₂
GaN:P ($5 \times 10^{14} \text{ cm}^{-2}$, 200KeV)	30 sec at 850 ⁰ C, in N ₂
GaN:P ($5 \times 10^{14} \text{ cm}^{-2}$, 200KeV)	45 sec at 850 ⁰ C, in N ₂
GaN:P ($5 \times 10^{14} \text{ cm}^{-2}$, 200KeV)	60 sec at 850 ⁰ C, in N ₂

C. Preliminary Results

Figure3-8 shows spectra of the near band gap luminescence of GaN undoped Fig.3-6 (from CREE and EMCORE) and Si doped Fig.7, 8 from CREE, excited by He-Cd laser (325nm) for different temperature. Cathodoluminescence spectra recorded at 5 KeV excitation energy shows a similar future.

Temperature dependence of the shorter wavelength peak of the PL of the three samples are shown in Fig. 9. For all sample curves b, c, d, Fig. 9 the PL lines we found a continuous decrease of the peak energy with increasing temperature T following the shift of the band gap curve "a," which is plotted using equation $E_g = 3.503 + (5.08 \times 10^{-4} T)/(T-996)$ eV.

It is well known that isoelectronic impurities in semiconductors produce bound states in the forbidden gap, binding an electron or a hole [1,2]. An isoelectronic center can form bound states because of a short range central-cell potential. According to Thomas [2,3] the primary factors affecting the binding potential are the electronegativity and the size differences between the impurity and the host ion which it replaces. It is found experimentally that only very large atoms or very small atoms produce isoelectronic traps because they create large lattice distortion induced by the substitution. Thomas, Robbins and Dean [2,3,4] have pointed out that to create a large binding potential, the substituted atom must generate a noticeable change in the local properties of the lattice. This is likely to produce an unfavorable free energy of solution, and hence a rather low solubility can be observed. For instance, the maximum concentration seen for bismuth in GaP was less than 10^{18} cm^{-3} [6]. Low solubility is also observed for rare earths in III-V semiconductors [5].

Allen [7] proposed different binding mechanisms for isoelectronic traps. According to Allen the isoelectronic impurity potential does not come from a pseudopotential difference of two isoelectronic atoms. Other possible sources are the spin orbit coupling, and the strain field in the close vicinity of the impurity due to the size difference between the impurity and the host atom which it replaces. The main results of his theory are that the perturbing potential at an isoelectronic impurity may be attracted simultaneously to both the electron and the holes, so bound exciton states can occur without bound single particle states. Baldereschi and Hopfield [8] have proposed a theory of isoelectronic traps assuming that the short range potential arises from core differences including spin orbit interaction between the dopant atom and the host atom it replaces. The relaxation of the host crystal around the impurity as well as the screening model considered appear to be important for the binding energy. However, discrepancies between experimental binding energies and those calculated from the differences in the atomic pseudopotentials are observed. The excellent reviews of existing theories and experimental data of isoelectronics impurities were given by Baldereschi [9] and Dean [5,10]. In GaP two isoelectronic traps have been extensively investigated; namely a nitrogen electron trap, and a

Figure 3

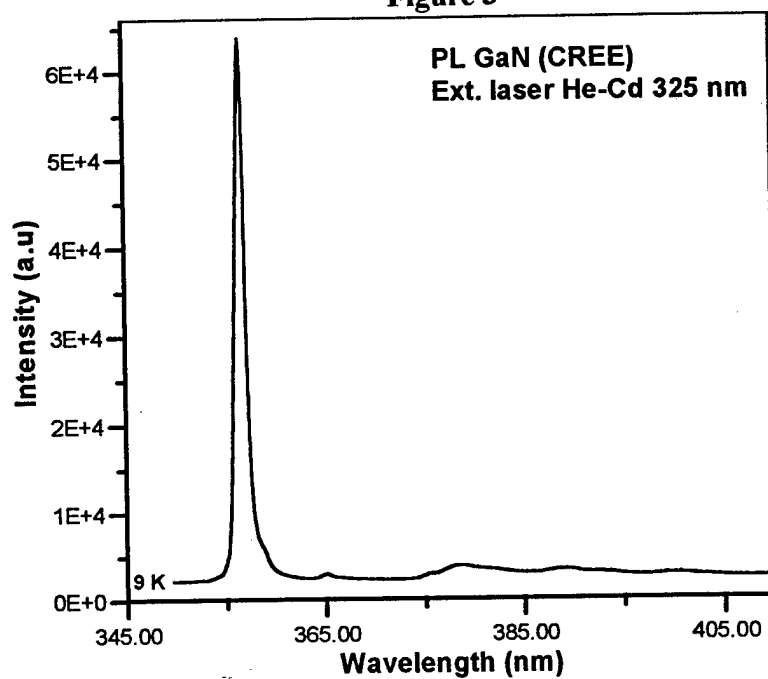


Figure 4

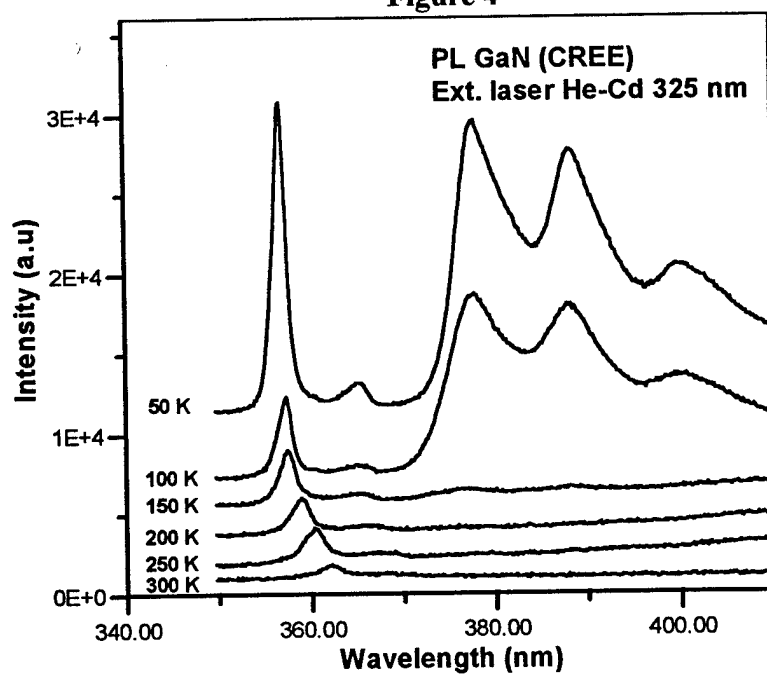


Fig.3 PL of MOCVD GaN (CREE) recorded at 9 K. Fig. 4 PL of GaN recorded at several temperatures, excited by He-Cd laser (325 nm, 30 mW).

Figure 5

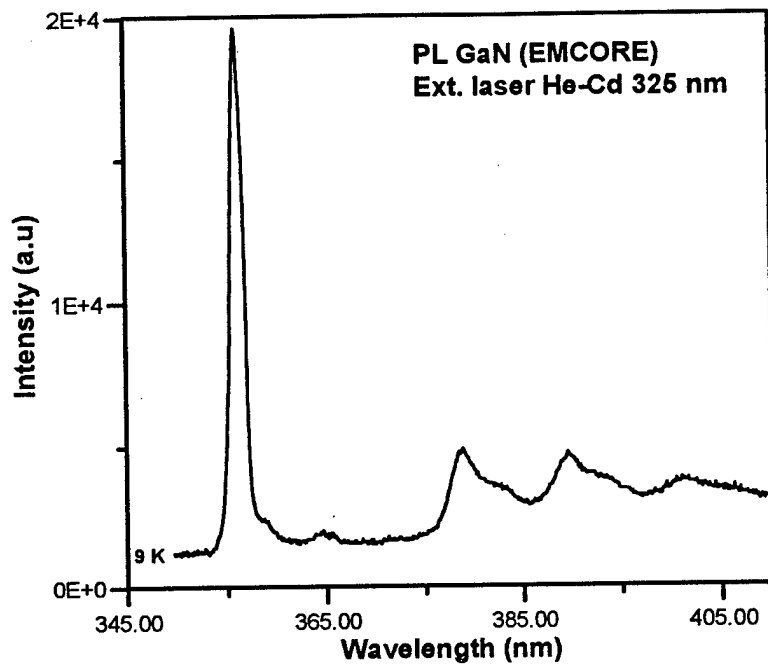


Figure 6

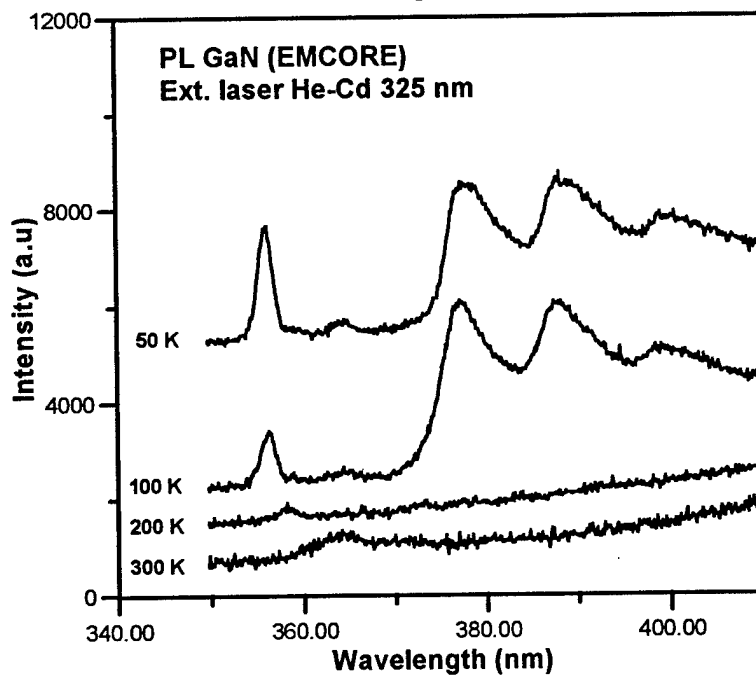


Fig 5,6 PL spectra at several temperatures of GaN (MOCVD), from EMCORE excited by He-Cd laser (325 nm, 30 mW).

Figure 7

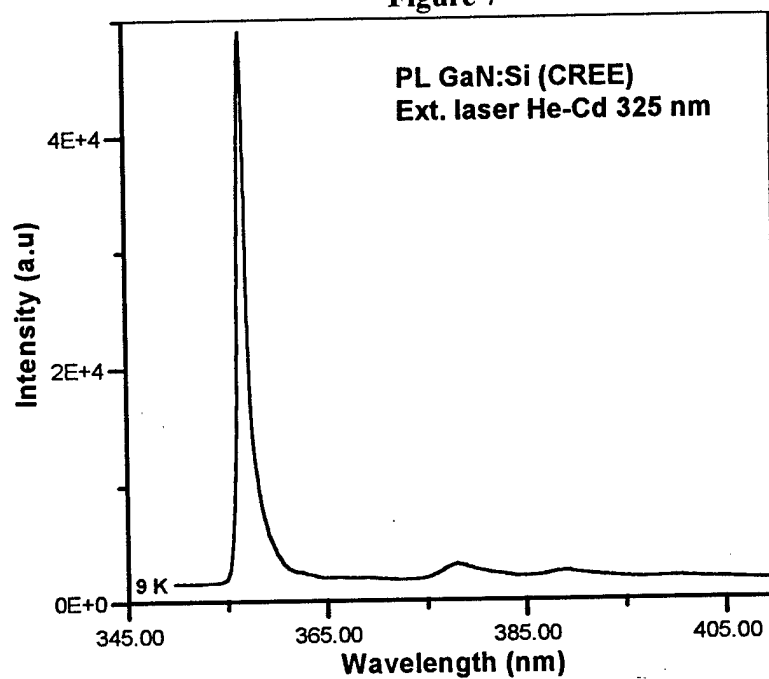


Figure 8

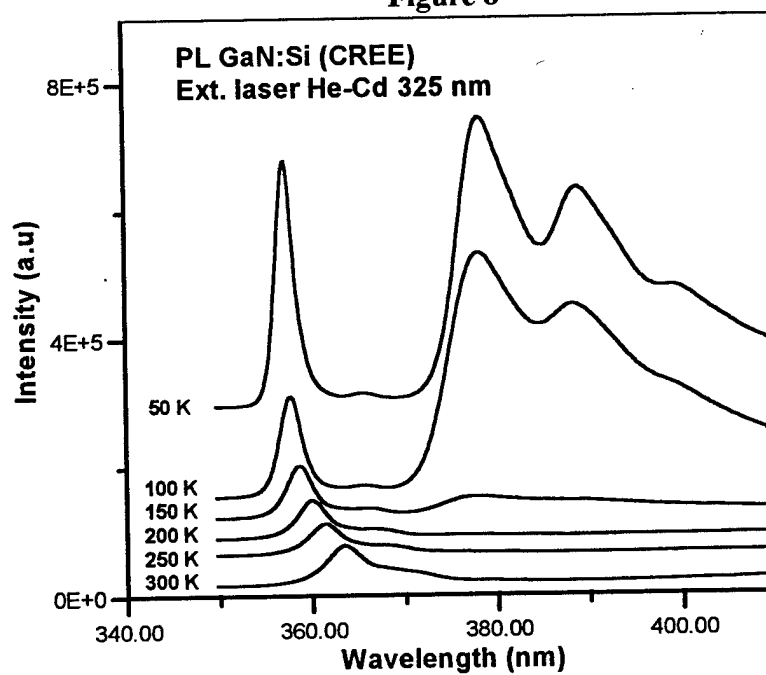


Fig.7,8 PL spectra of MOCVD GaN: Si (6×10^{17}) from CREE recorded at several temperatures, excited by He-Cd laser (325 nm, 30mW).

bismuth hole trap formed by substituting Bi and N for phosphorus [5]. In the direct band-gap III-V semiconductors isoelectronic impurities have been investigated only in InP doped with bismuth [11,12]. The neutral Bi, in a P site, creates a hole trap, and the isoelectronic complex (Bi,X)-(Bi,X) bound-excitonic molecules [12]. In II-VI semiconductors, ZnTe doped with oxygen-electron traps and CdS doped with tellurium hole-traps were investigated in detail [10].

It is noticeable that all isoelectronic impurities discussed above involve substitutions on the anion sites. The previous investigation [13] of cationic isoelectronic substituent (Mg, Ca, Sr, Ba) in ZnSe and ZnTe found no evidence for the presence of isoelectronic traps. A strong photoluminescence (PL) was reported recently from Mg doped ZnSe [14a,b] and ZnS [15] which may arise from a new isoelectronic center generated by magnesium. We observed [14] sharp emission with a half-width of 16-30 meV (for $\text{Mg}_x\text{Zn}_{1-x}\text{Se}$ $x=0.04$), as required for exciton transitions at low temperatures. Furthermore the PL characteristics shift dramatically from deeper extrinsic emission in ZnSe to be dominated by narrow near bandgap emission at all temperatures in the range 2-300 K in $\text{Mg}_{0.04}\text{Zn}_{0.96}\text{Se}$. The temperature dependence of the energy position of this peak follows the expected behavior for a free exciton transition in ZnSe. This peak remains strong in the PL spectrum all the way up to room temperature. This kind of behavior is not usually observed for bound exciton transitions related to neutral donor or acceptor centers. However this behavior is typical for excitons bound to isoelectronic traps for which the dominant decay mode is radiative. The presence of the third electronic particle in the first two cases, but not in the third, was shown to introduce a dominant Auger decay mode for the bound exciton. In the Auger quenching, all the recombination energy is transferred to this third electronic particle that is expelled deep into the conduction band (electron) or valence band (hole) respectively.

In relation with the above review of an isoelectronic trap in different semiconductors we started the investigation of an effect of the implantation of possible isoelectronic group V impurity, phosphorus, upon the luminescence from GaN. The most natural candidate is phosphorus (P) replacing nitrogen in GaN. Replacing nitrogen by phosphorus in GaN should create an isoelectronic trap similar too extensively an investigated nitrogen electron trap in GaP [5]. Bismuth substituted for phosphorus is a hole trap in GaP. Similarly by substituting Bi for nitrogen in GaN can create the hole trap. Table III and Fig.2 are summarizing the implantation and annealing conditions. The beam was inclined at 7° to the normal to the GaN layers to prevent channeling along preferred crystallographic directions.

Figure 9

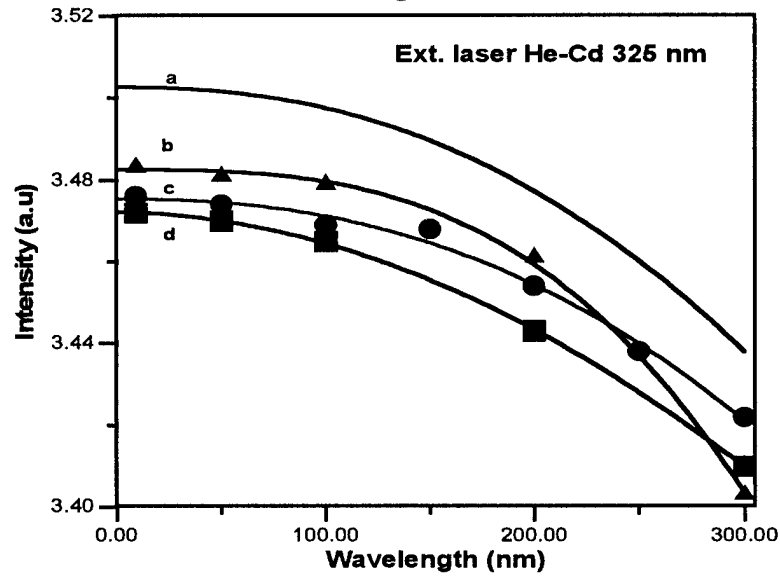


Figure 10

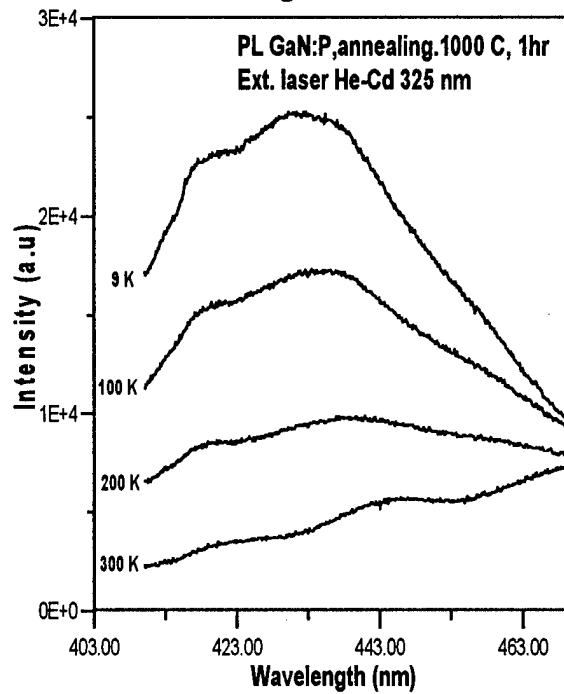


Fig. 9 Temperature dependence of the short wavelength peak: for a sample from Fig.3, 4 curve b; for a sample from Fig. 5,6 curve c; for a sample from Fig.7, 8 curve d, and the band gap shift plotted using equation: $E_g = 3.503 + (5.08 \times 10^{-4} T)/(T-996)$ eV. Fig. 10 PL of GaN: P at several temperatures, excited by He-Cd laser (325 nm, 30 mW).

The samples were at room temperature. The profiles were calculated using Ion beam profile code V. 3.20 software. The maximum accelerating potential in the system was 200 keV, used for the P^+ ions, giving a mean projected range of 163.7 nm. The ion flux rates were $5 \times 10^{14} \text{ cm}^{-2}$, which gives the maximum concentration of P at peak of the Pearson profile to be $3.31 \times 10^{19} \text{ cm}^{-3}$ as seen in Fig.2. Each nuclear collision produces a knocked on target atoms, which in turn products a cascade of secondary collisions, giving rise to a highly damaged small volume which may be amorphous in nature. However, much of the damage appears to be removed by self-annealing. Despite it, residual damages are still high enough to quench luminescence, which recovered by annealing at elevated temperatures in NH_3 to prevent N loss from the GaN. The spectra were excited by He-Cd laser (325 nm), and analysed using a scanning monochromator ISA HR320 with greating 600g/mm, and TEA/CCD- 512-TKBM1 high sensitivity CCD detector from Princeton Instruments Inc.

Preliminary measurements had indicated the broad nature of the luminescence features. The PL bands near 2.98 eV and 2.88 eV appeared with implanted P^+ impurity, and must be associated with the presence of these impurities in the system. The energies indicate impurity levels about 0.52eV and 0.62 eV from the band edges, rather than the shallow isoelectronic traps observed in GaP for example [5]. However, these preliminary experimental results do not allow a detailed description of the nature of the impurity centres or the radiative transitions.

1. A. C. Aten, J. H. Haanstra and H. de Vries, Philips Research Reports, 20, 395, (1965).
2. D. G. Thomas, J. J. Hopfield and C. J. Frosch, Phys Rev. Lett. 15, 857, (1965).
3. D. G. Thomas, J. of the Phys. Soc. of Japan, 21, 265 (1966).
4. D. J. Robbins and P. J. Dean, Adv. in Physics, 27 (4), 499 (1978) and references therein.
5. P. J. Dean, J. of Lumin., 7, 51, (1973).
6. H. C. Casey Jr., and G. L. Pearson, J. Appl. Phys. 35, 3401, (1964).
7. J. W. Allen, J. Phys. C: Solid State Phys., 4, 1936, (1971).
8. A. Baldereschi and J.J. Hopfield, Phys. Rev. Lett. 28, 171, (1972)
9. A. Baldereschi, J. of Lumin., 7, 79, (1973).

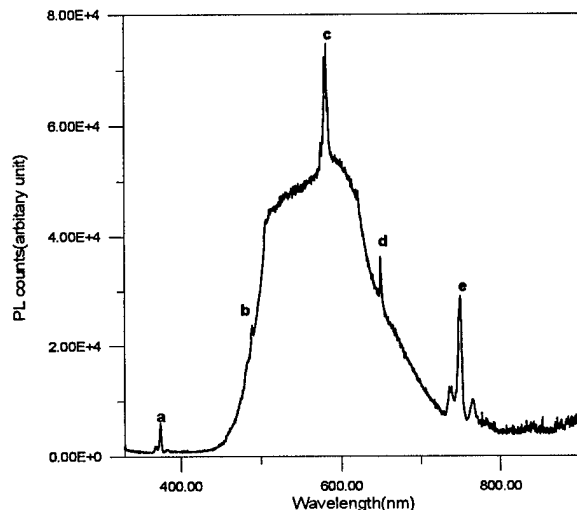
10. W. Czaja, Advances in Solid State Physics XI, edited by O. Madelung, Pergamon Press, 65(1971) and references therein.
11. P. J. Dean, A. M. White, E. W. Williams, and M. G. Astles, Solid State Commun. 9, 1555, (1971).
12. W. Ruhle, W. Schmid, R. Meck, N. Stath, J. U. Fischbach, I. Strottner, K. W. Benz, and M. Pilkuhn, Phys. Rev. B, 18 (12), 7022, (1978).
13. J.L. Merz, and R. T. Lynch., II-VI Semiconducting Compounds, edited by D. G. Thomas (New York: W. A. Benjamin Inc.) p.730, (1967).
14. a) H.J. Lozykowski, P.O. Holtz, and B. Monemar, J. of Electronic Materials, 12, 653, (1983), b) H. J. Lozykowski, and J. L. Merz, Mat. Res. Soc. Symp. Proc. Vol. 161, 171, (1990).
15. T. R. N. Kutty and R. Revathi, Solid State Commun. 55, 197, (1985).

III PREPARATION OF POLYCRYSTALLINE GaN, AND ZNO PHOSPHORS DOPED WITH RARE EARTH AND OTHERS IMPURITIES

In this chapter, preliminary results of luminescence investigations of pure and rare earth (RE) doped single crystals and microcrystalline powders of GaN, ZnO, and sintered pellets of GaN, and ZnO. The GaN single crystals were grown using method describes by Zetterstrom [1] and Ogino [2]. The starting material was gallium nitride powder 3-9' s pure, or Ga₂O₃ 5-9's from Cerac Inc. The quartz boat was in quartz liner and inserted into a quartz tube and heated in a stream of ammonia. Needle single crystals ~ 4 mm long and 10- 30 μ m in diameter was growth at temperature 1170⁰ C in 72 h period. Some of the crystals are transparent and some black needles. The darkening of the GaN is probably due to nitrogen vacancies [2,3]. The synthesis of microcrystal GaN powders was prepared using 5-9's pure Ga₂O₃ powder from Cerac Inc. The motivation to investigate GaN microcrystal powder was simplicity of preparation and low cost. GaN powder is much cheaper than thin film GaN crystals. Investigation of luminescence properties of needles crystals and microcrystal GaN powders doped with

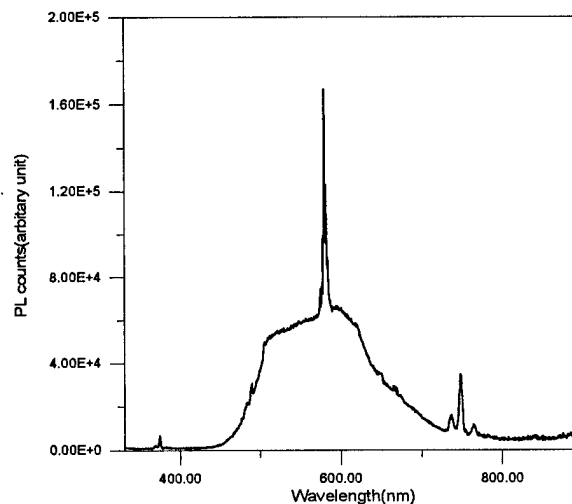
rare earth is in progress. The results obtained on microcrystalline samples can be implemented to synthesis monocrystalline layers. Inspiration for the study of luminescence properties of ZnO doped with RE is that ZnO is one of the most suitable hexagonal substrates with the best matching lattice constant for gallium nitride growth. The bandgap energy of ZnO is 3.2 eV, and wurtzite GaN is 3.39 eV at 300K. The heterojunction between n-type ZnO and p-type GaN can play an important role in new light emitting devices. Investigation's photoluminescence of ZnO doped with rare earth is important from the application point of view, and can provide important information about a role of oxygen in co-doping with rare earth in GaN and other nitrides. The preliminary results are promising, we obtained for the first time ever strong photoluminescence emission at room temperature from ZnO doped with Dy, Er, Tm, Ho, Nd, and co-doped with Li, Na, and F. The examples of photoluminescence spectra obtained under above and below bandgap excitations using He-Cd (325 nm), and argon ion laser lines at different temperatures are shown on Figures 11-30 for ZnO: Dy, Li. Figures 31-50 shown the photoluminescence spectra obtained under below bandgap excitations using argon ion laser lines at different temperatures for ZnO: Er, Li. The example of PL spectra of ZnO: Tm, Li. obtained under above and below bandgap excitations using He-Cd (325 nm) and argon ion laser lines at 9K and 100K temperatures are shown on Figures 51-54. We also investigate the cathodoluminescence (CL) excited by an electron beam from an electrostatically focused Electroscan EG5 VSW electron gun giving the acceleration potentials within the range from 1 kV to 5 kV. The samples for PL and CL study were mounted on the cold finger of a Model LTS 22-1 closed cycles cryogenic refrigerator system covering the temperature range 8 -300 K. The tentative assignment for observed Dy, Er, and Tm emission transitions is shown in the figures captions.

Figures 55, 56 shows' example of the PL rise and decay kinetics of transition $^4F_{9/2} \rightarrow ^6H_{13/2}$ for ZnO: Dy, Li excited at two different wavelengths 457.9 nm and 476.5 nm with power 80 mW. Figures 57, 58, show the PL rise and decay kinetics of $^4H_{11/2} \rightarrow ^4I_{15/2}$ transition for ZnO: Er, Li excited at two different wavelength 488 nm and 514.5 nm respectively with power 80 mW. Figures 55-58 shows also the excitation laser pulses. The rise and decay times obtained from fitting to double exponential function are shown in Table V. The kinetics study was done, using an acousto-optical light modulator (IntraAction model AOM-125), and turbo-multichannel scaler (Turbo-MCS EG&G Ortec), which offers a wide range of channel dwell times (minimum 5 ns), with no dead time between channels.



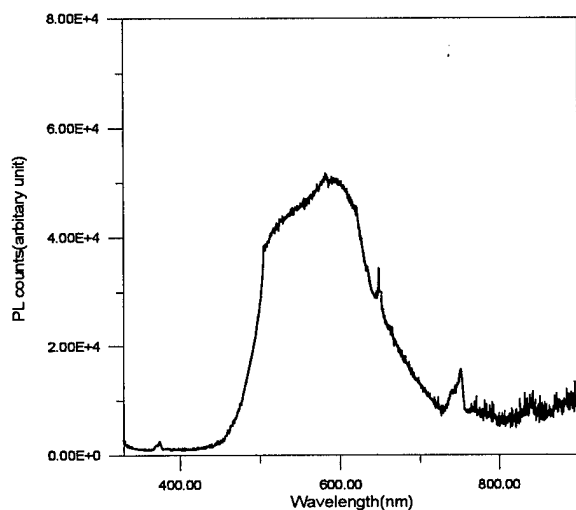
PL of ZnO:Dy with Li at T=10K,
exec@325nm, 30mW

Figure 11



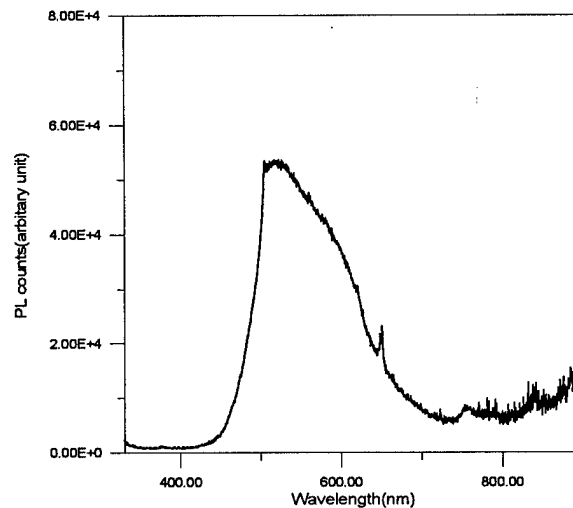
PL of ZnO:Dy with Li at T=50K,
exec@325nm, 30mW
(Note that the scale is different from others)

Figure 12



PL of ZnO:Dy with Li at T=150K,
exec@325nm, 30mW

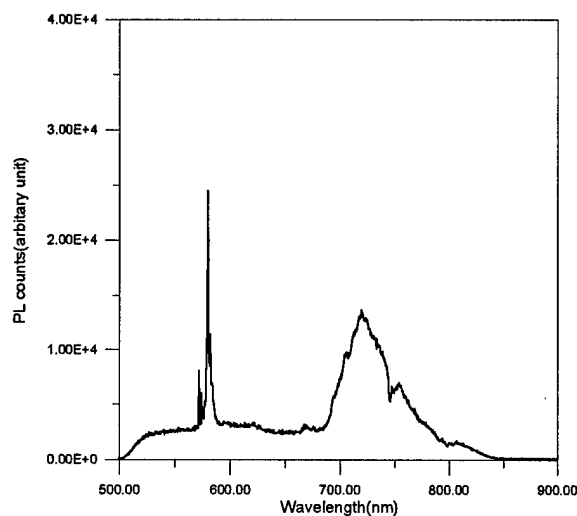
Figure 13



PL of ZnO:Dy with Li at T=250K,
exec@325nm, 30mW

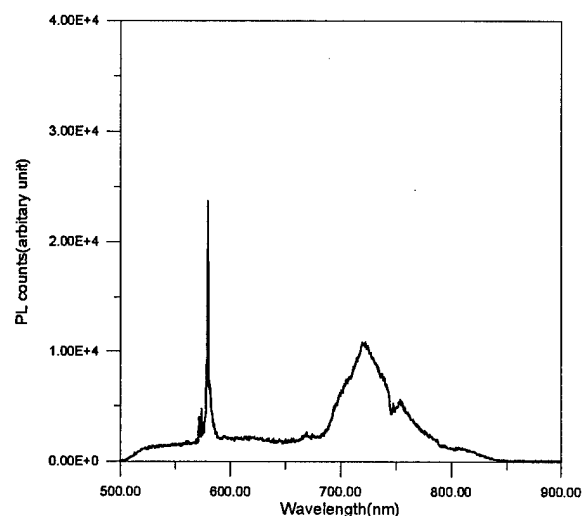
Figure 14

Figures 11-14: shows the PL spectra of ZnO: Dy, Li excited by He-Cd laser (325nm, 30 mW) recorded at 10, 50, 150 and 250 K. The spectra on Fig.11 contained the wide band host lattice emission overlapping with peaks: a at ~ 375 nm is assigned tentatively to transition ${}^4G_{11/2} \rightarrow {}^6H_{15/2}$, b at ~ 490 nm is assigned to transition ${}^4F_{9/2} \rightarrow {}^6H_{15/2}$, peak c at ~582 nm is assigned to transition ${}^4F_{9/2} \rightarrow {}^6H_{13/2}$, peak d at ~749 nm is assigned to transition ${}^4F_{9/2} \rightarrow {}^6H_{9/2}$. Peak d is the II order laser line.



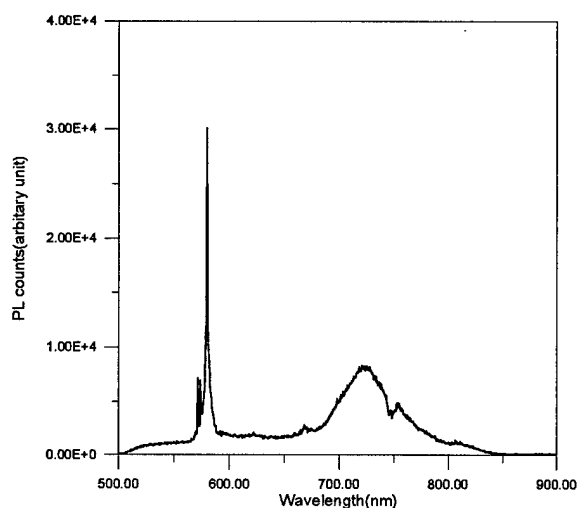
PL of ZnO:Dy with Li at T=10K,
exec@457.9nm, 200mW

Figure 15



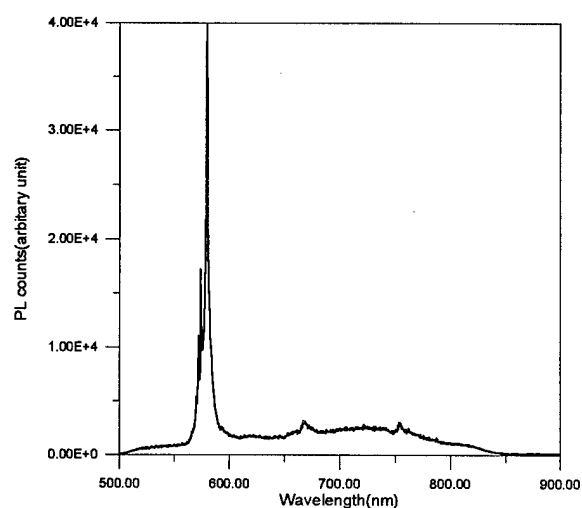
PL of ZnO:Dy with Li at T=100K,
exec@457.5nm, 200mW

Figure 16



PL of ZnO:Dy with Li at T=150K,
exec@457.9nm, 200mW

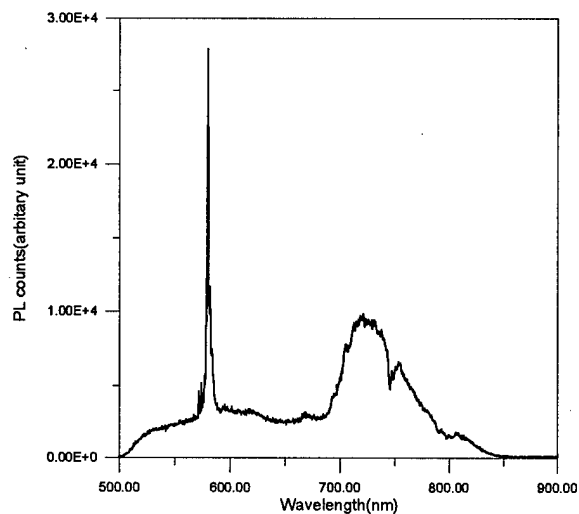
Figure 17



PL of ZnO:Dy with Li at T=250K,
exec@457.9nm, 200mW

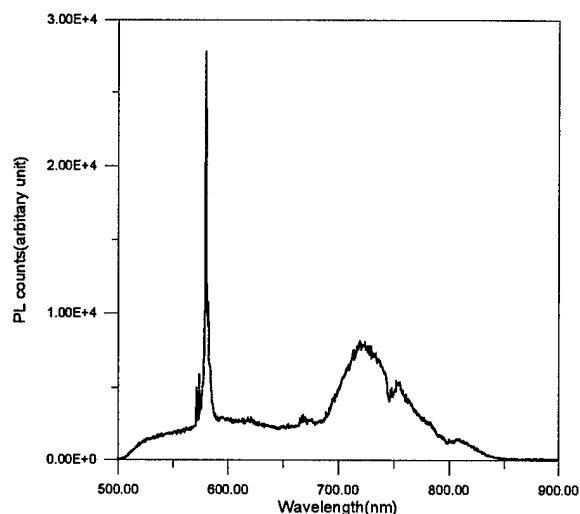
Figure 18

Figure 15-18: shows the PL spectra of ZnO: Dy, Li excited by Ar^+ laser line at 457.5 nm, (200 mW) recorded at 10, 100, 150 and 250 K. The spectra on Fig.15 contained the wide band emission overlapping with dominant peak at $\sim 574\text{-}580$ nm assigned to transition ${}^4\text{F}_{9/2} \rightarrow {}^6\text{H}_{13/2}$. We also can see peaks at 669nm, 705nm, 720nm 760nm (the last two are assigned to transition ${}^4\text{F}_{9/2} \rightarrow {}^6\text{H}_{9/2}$), and 809nm.



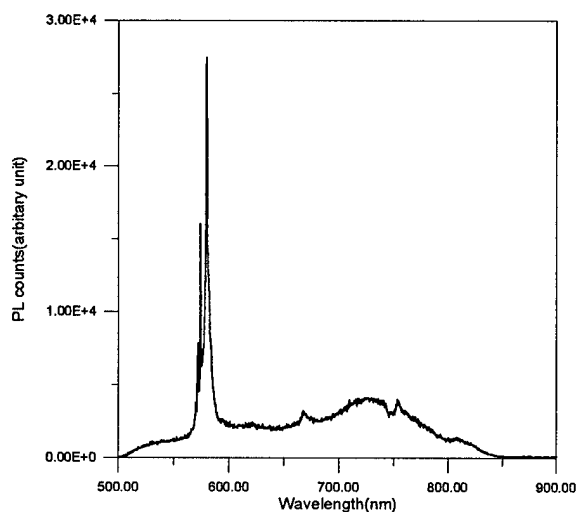
PL of ZnO:Dy with Li at T=10K,
exec@476.5nm, 200mW

Figure 19



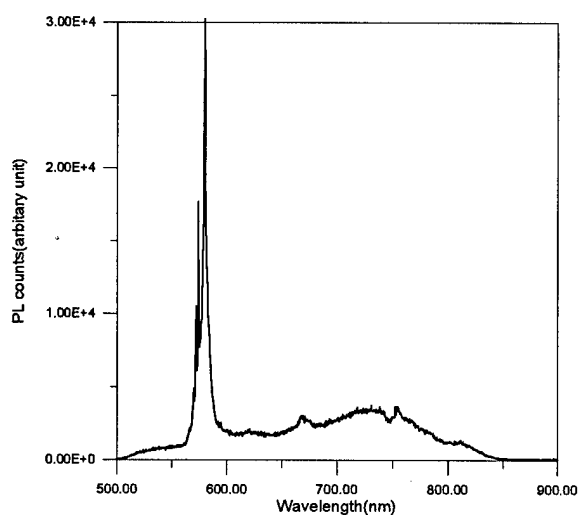
PL of ZnO:Dy with Li at T=100K,
exec@476.5nm, 200mW

Figure 20



PL of ZnO:Dy with Li at T=200K,
exec@476.5nm, 200mW

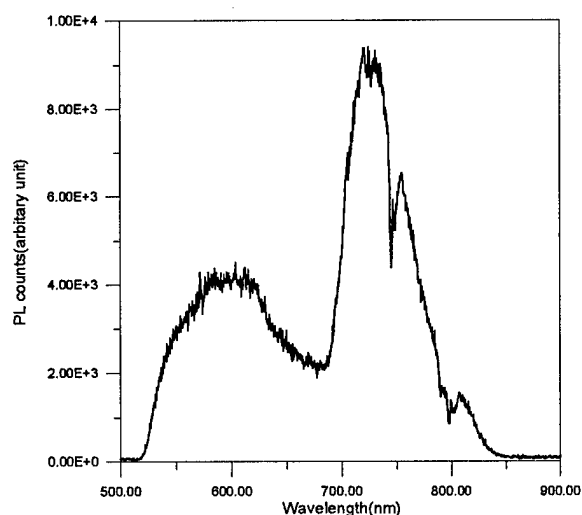
Figure 21



PL of ZnO:Dy with Li at T=250K,
exec@476.5nm, 200mW

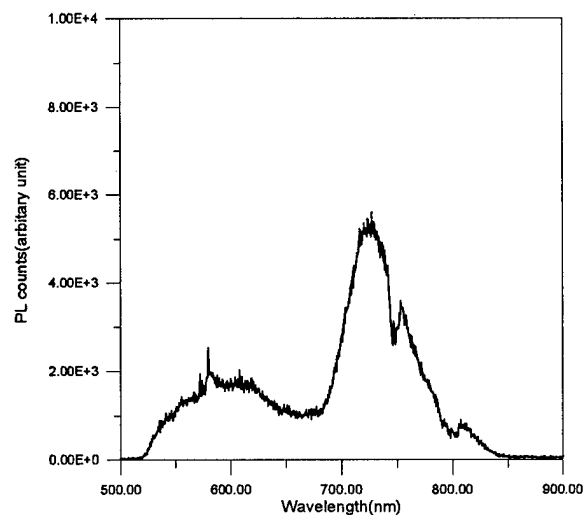
Figure 22

Figure 19-22: shows the PL spectra of ZnO: Dy, Li excited by Ar^+ laser line at 476.5 nm, (200 mW) recorded at 10, 100, 200 and 250 K. The spectra at Fig. 22 shows, the wide band emission overlapping with dominant peak at ~ 580 nm assigned to transition $^4F_{9/2} \rightarrow ^6H_{13/2}$, and peaks at 622nm, 669nm, 731nm, 754nm and 811nm.



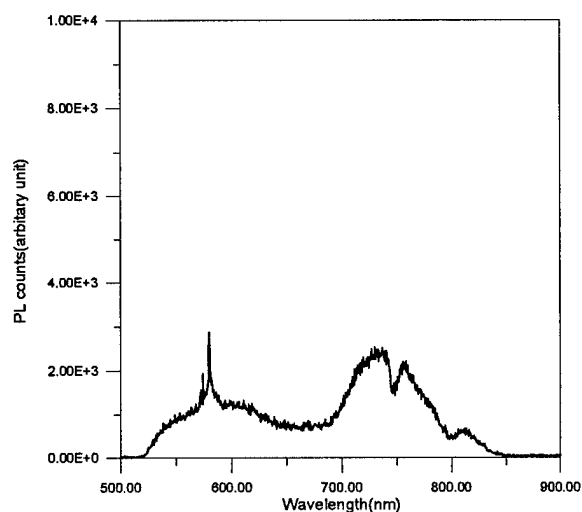
PL of ZnO:Dy with Li at T=10K,
exec@488.0nm, 200mW

Figure 23



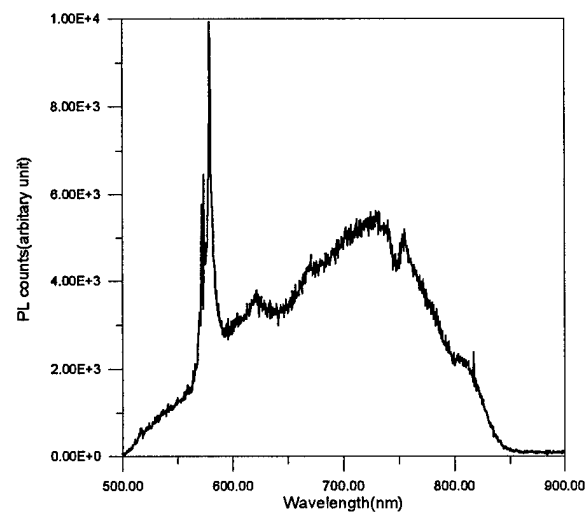
PL of ZnO:Dy with Li at T=150K,
exec@488.0nm, 200mW

Figure 24



PL of ZnO:Dy with Li at T=200K,
exec@488.0nm, 200mW

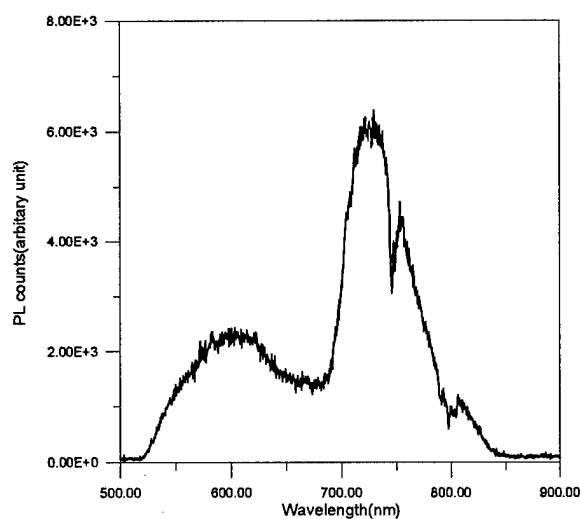
Figure 25



PL of ZnO:Dy with Li at T=300K,
exec@488.0nm, 200mW

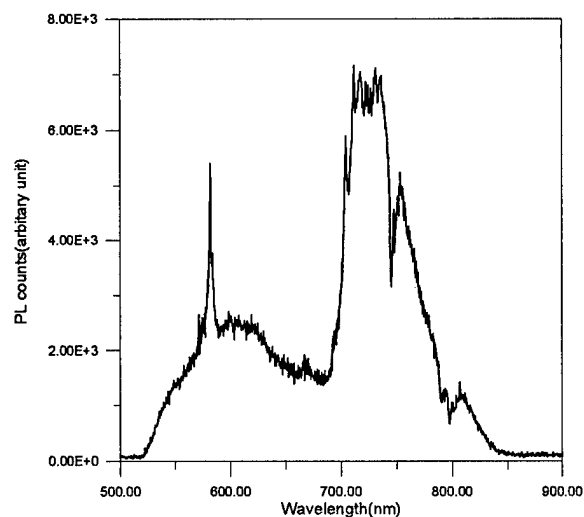
Figure 26

Figure 23-26: shows the PL spectra of ZnO: Dy, Li excited by Ar^+ laser line at 488 nm, (200 mW) recorded at 10, 150, 200 and 300 K. The room temperature (300K) spectrum contained the wide band emission overlapping with dominant peak at ~ 579 nm assigned to transition $^4\text{F}_{9/2} \rightarrow ^6\text{H}_{13/2}$, and peaks at 621nm, 669nm, 727nm, 755nm, and 808nm.



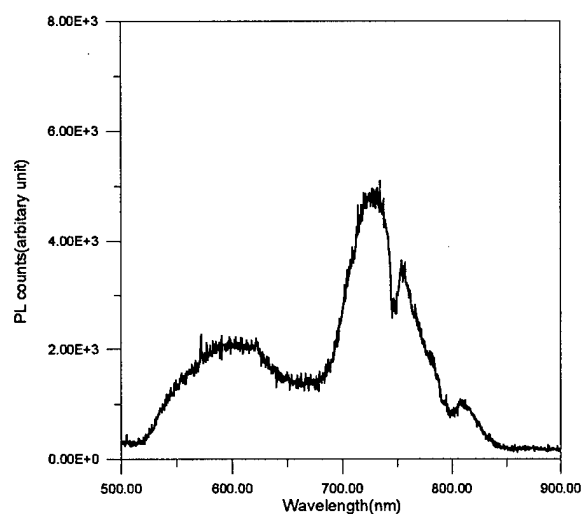
PL of ZnO:Dy with Li at T=10K,
exec@496.5nm, 200mW

Figure 27



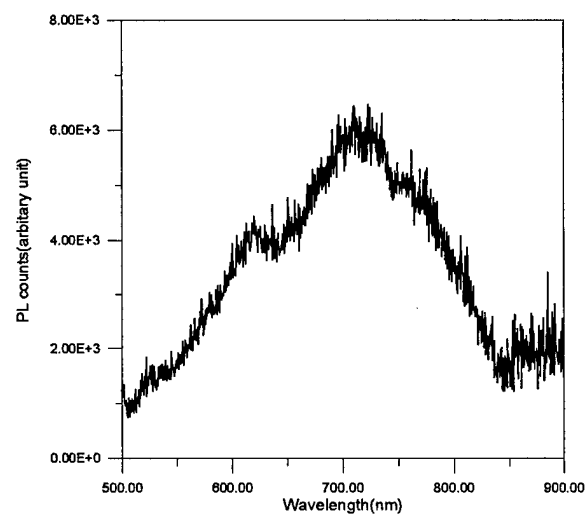
PL of ZnO:Dy with Li at T=50K,
exec@496.5nm, 200mW

Figure 28



PL of ZnO:Dy with Li at T=150K,
exec@496.5nm, 200mW

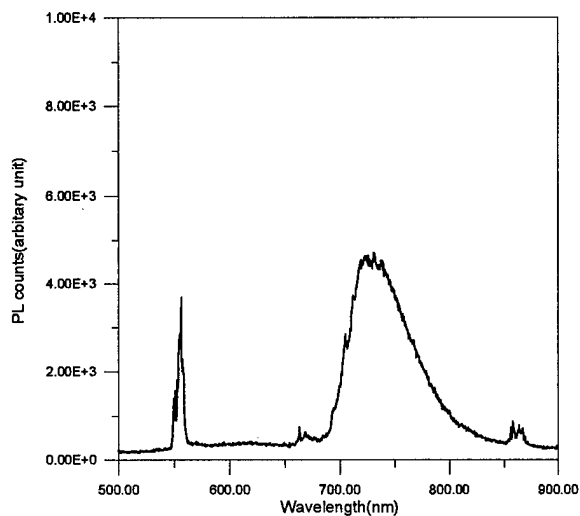
Figure 29



PL of ZnO:Dy with Li at T=300K,
exec@496.5nm, 200mW

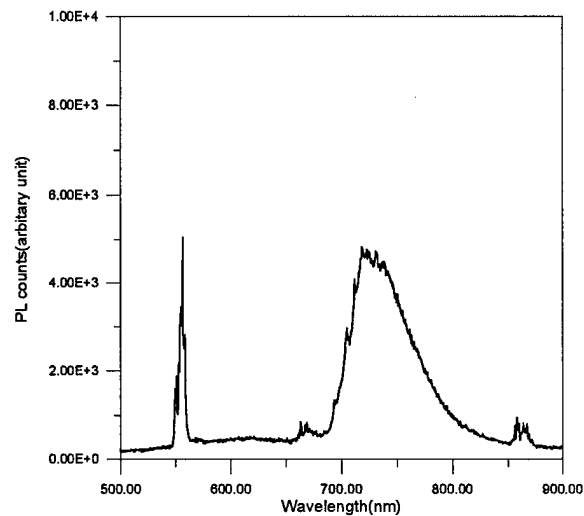
Figure 30

Figure 27-30: shows the PL spectra of ZnO: Dy, Li excited by Ar⁺ laser line at 496.5 nm, (200 mW) recorded at 10, 50, 150 and 300 K. The spectra at Fig. 28 showed the wide bands emission and several sharp peaks at 582nm (transition ${}^4F_{9/2} \rightarrow {}^6H_{13/2}$), 705nm, 722-755nm (transition ${}^4F_{9/2} \rightarrow {}^6H_{9/2}$), and 809nm.



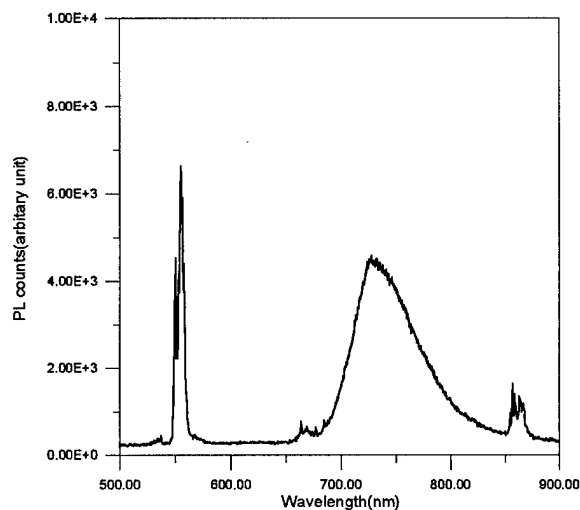
PL of ZnO:Er with Li at T=10K,
exec@457.9nm, 200mW

Figure 31



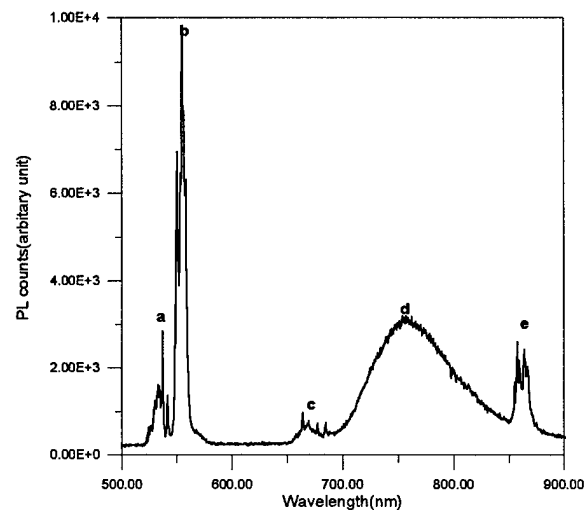
PL of ZnO:Er with Li at T=50K,
exec@457.9nm, 200mW

Figure 32



PL of ZnO:Er with Li at T=150K,
exec@457.9nm, 200mW

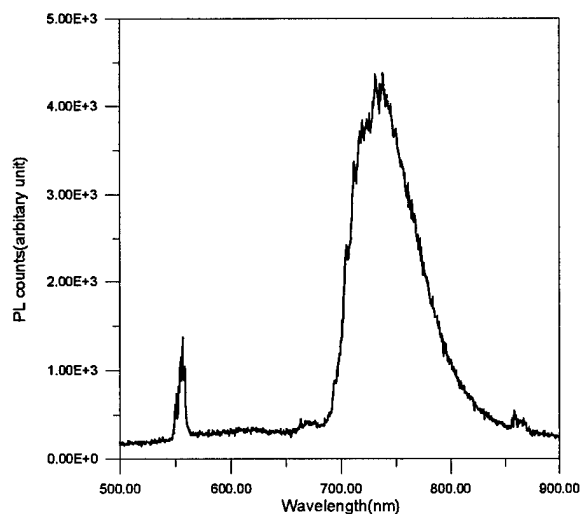
Figure 33



PL of ZnO:Er with Li at T=250K,
exec@457.9nm, 200mW

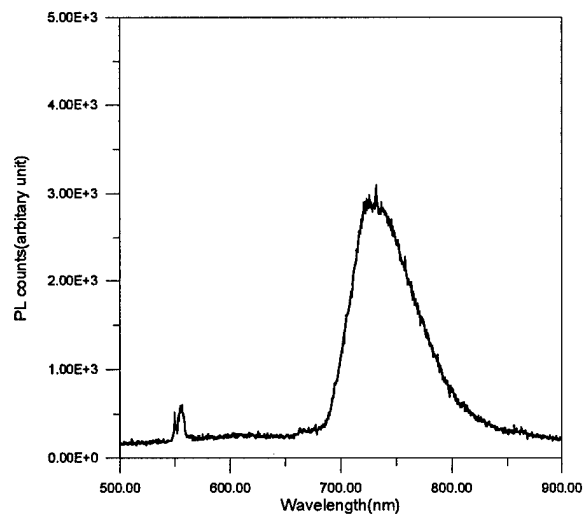
Figure 34

Figure 31-34: shows the PL spectra of ZnO: Er, Li excited by Ar^+ laser line at 457.9 nm, (200 mW) recorded at 10, 50, 150 and 250 K. The spectra on Fig. 34 shows Er^{3+} emission at 250K, the peaks a at ~540 nm assigned to transition $^4\text{H}_{11/2} \rightarrow ^4\text{I}_{15/2}$, the dominant peaks b at 555 nm assigned to transition $^4\text{S}_{3/2} \rightarrow ^4\text{I}_{15/2}$, peaks c at 667 nm ($^4\text{F}_{9/2} \rightarrow ^4\text{I}_{5/2}$), wide band d at ~770 nm ($^4\text{I}_2 \rightarrow ^4\text{I}_{5/2}$), and peaks e at 862 nm ($^4\text{S}_{3/2} \rightarrow ^4\text{I}_{13/2}$).



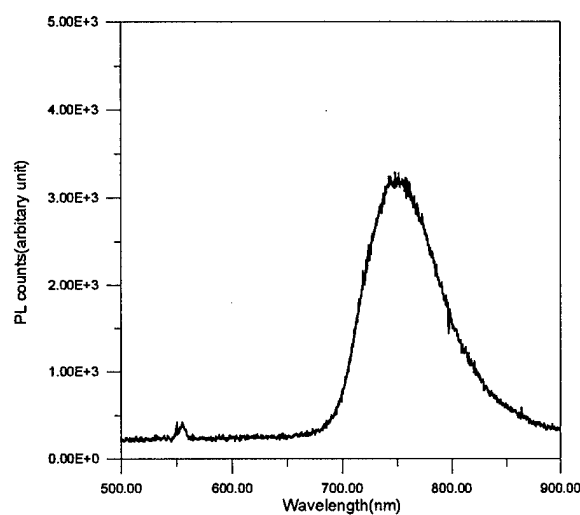
PL of ZnO:Er with Li at T=10K,
exec@476.5nm, 200mW

Figure 35



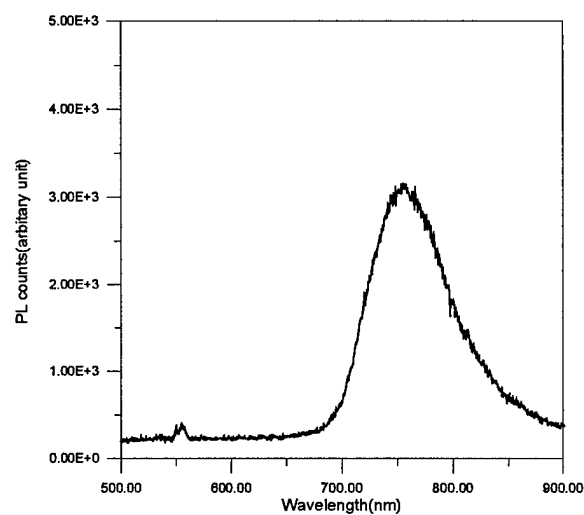
PL of ZnO:Er with Li at T=100K,
exec@476.5nm, 200mW

Figure 36



PL of ZnO:Er with Li at T=200K,
exec@476.5nm, 200mW

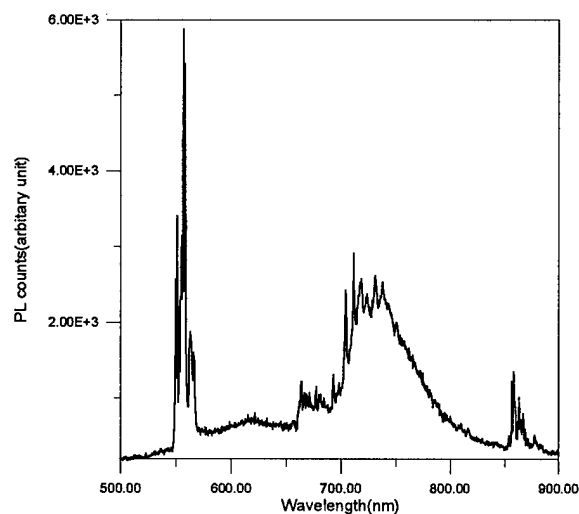
Figure 37



PL of ZnO:Er with Li at T=250K,
exec@476.5nm, 200mW

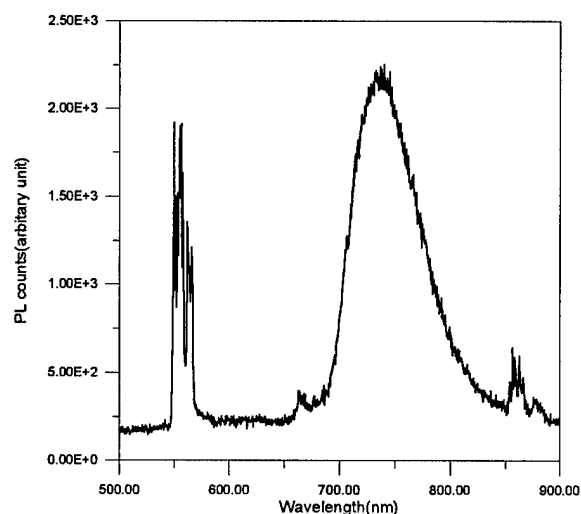
Figure 38

Figure 35-38: shows the PL spectra of ZnO: Er, Li excited by Ar^+ laser line at 476.5 nm, (200 mW) recorded at 10, 100, 200 and 250 K. The spectra on Fig. 35 shows Er^{3+} emission at 10K, the peaks at 556nm, ~669nm, ~705-770nm, and 862nm are assigned to transitions: $^4\text{S}_{3/2} \rightarrow ^4\text{I}_{15/2}$, $^4\text{F}_{9/2} \rightarrow ^4\text{I}_{15/2}$, $^4\text{I}_{9/2} \rightarrow ^4\text{I}_{15/2}$, and $^4\text{S}_{3/2} \rightarrow ^4\text{I}_{13/2}$ respectively.



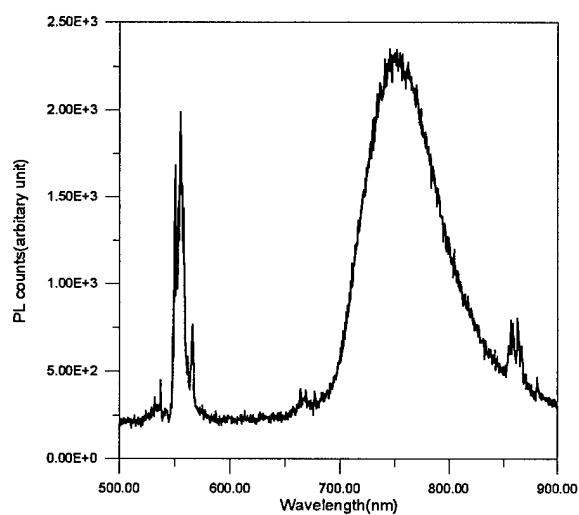
PL of ZnO:Er with Li at T=10K,
exec@488.0nm, 200mW

Figure 39



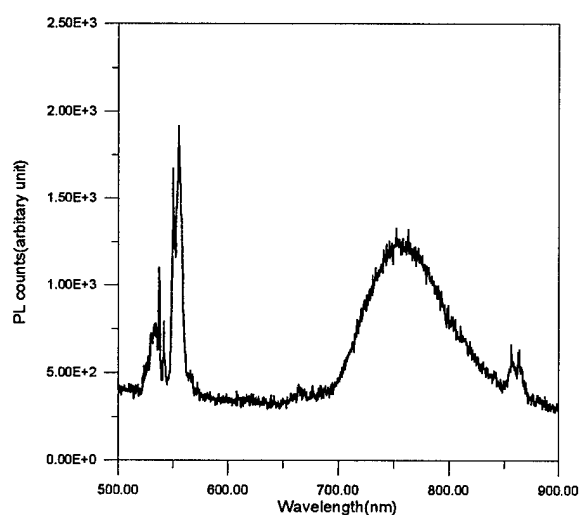
PL of ZnO:Er with Li at T=100K,
exec@488.0nm, 200mW

Figure 40



PL of ZnO:Er with Li at T=200K,
exec@488.0nm, 200mW

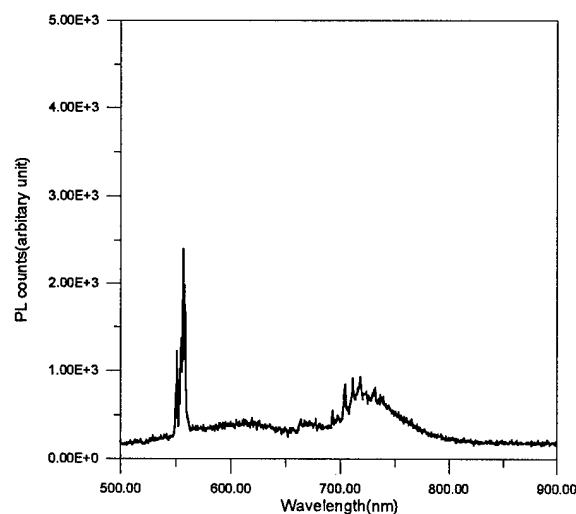
Figure 41



PL of ZnO:Er with Li at T=300K,
exec@488.0nm, 205mW

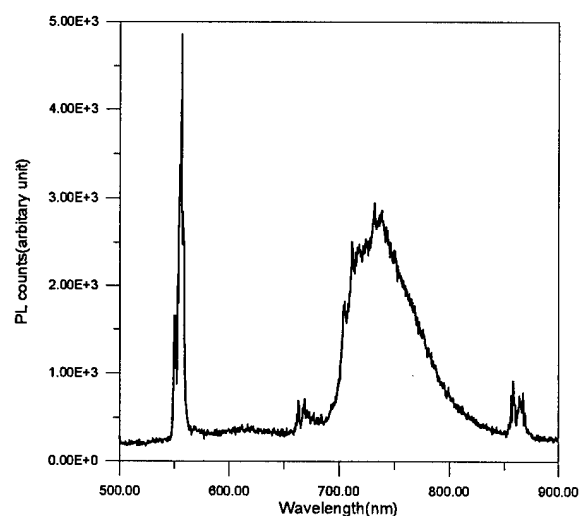
Figure 42

Figure 39-42: shows the PL spectra of ZnO: Er, Li excited by Ar^+ laser line at 488 nm, (200 mW) recorded at 10, 100, 200 and 250 K. The spectra on Fig. 39 shows Er^{3+} emission at 10K, the dominant peak at 556nm assigned to transition $^4\text{S}_{3/2} \rightarrow ^4\text{I}_{15/2}$, the remaining peaks have assignment as in Fig.35.



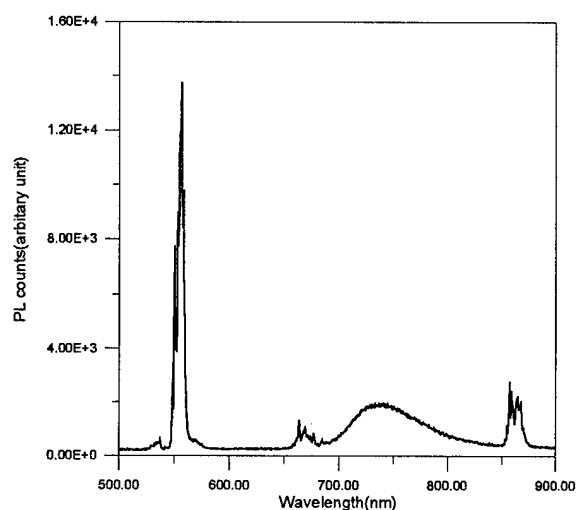
PL of ZnO:Er with Li at T=10K,
exec@496.5nm, 197mW

Figure 43



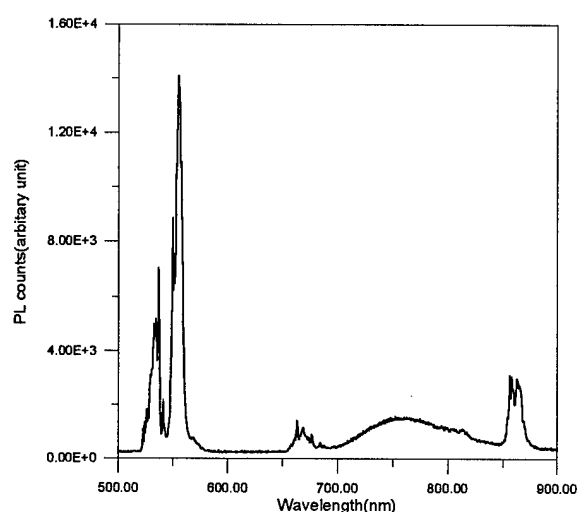
PL of ZnO:Er with Li at T=50K,
exec@496.5nm, 200mW

Figure 44



PL of ZnO:Er with Li at T=150K,
exec@496.5nm, 200mW

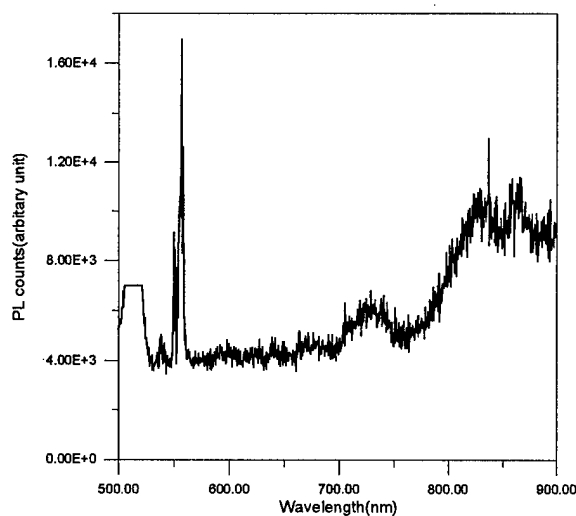
Figure 45



PL of ZnO:Er with Li at T=300K,
exec@496.5nm, 205mW

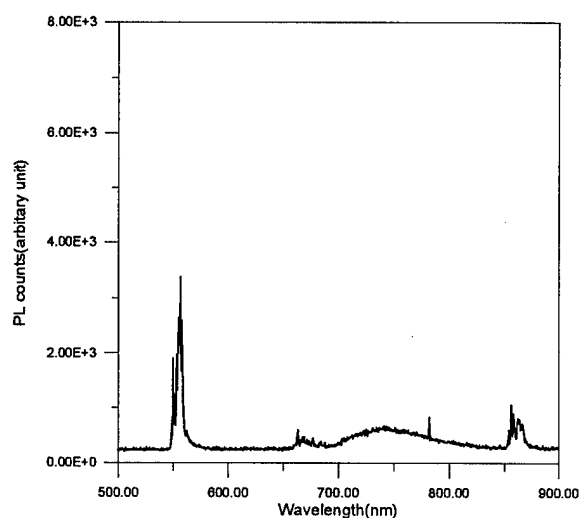
Figure 46

Figure 43-46: shows the PL spectra of ZnO: Er, Li excited by Ar^+ laser line at 457.9 nm, (200 mW) recorded at 10, 50, 150 and 300 K. The spectra on Fig. 46 shows Er^{3+} emission at 300K, the peaks at ~ 540 nm assigned to transition $^4\text{H}_{11/2} \rightarrow ^4\text{I}_{15/2}$, the dominant peaks at 555 nm assigned to transition $^4\text{S}_{3/2} \rightarrow ^4\text{I}_{15/2}$, peaks at 667 nm ($^4\text{F}_{9/2} \rightarrow ^4\text{I}_{15/2}$), a wide band at $\sim 757\text{--}815$ nm ($^4\text{I}_2 \rightarrow ^4\text{I}_{13/2}$), and peaks at 857 nm ($^4\text{S}_{3/2} \rightarrow ^4\text{I}_{13/2}$).



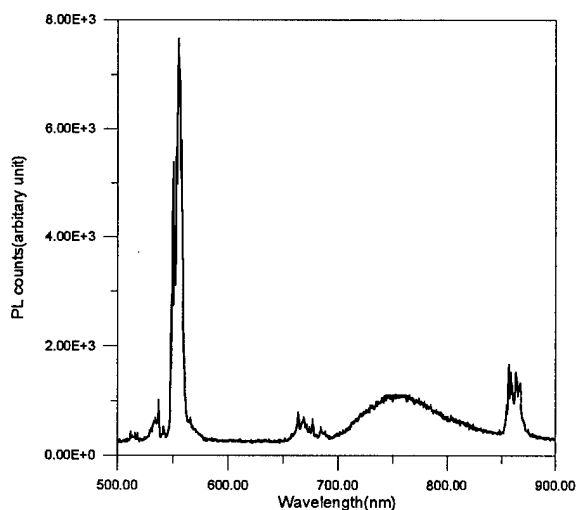
PL of ZnO:Er with Li at T=10K,
exec@514.5nm, 200mW

Figure 47



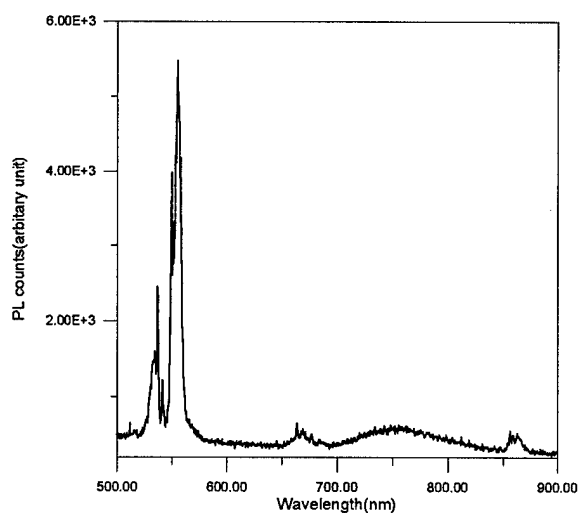
PL of ZnO:Er with Li at T=100K,
exec@514.5nm, 200mW

Figure 48



PL of ZnO:Er with Li at T=200K,
exec@514.5nm, 200mW

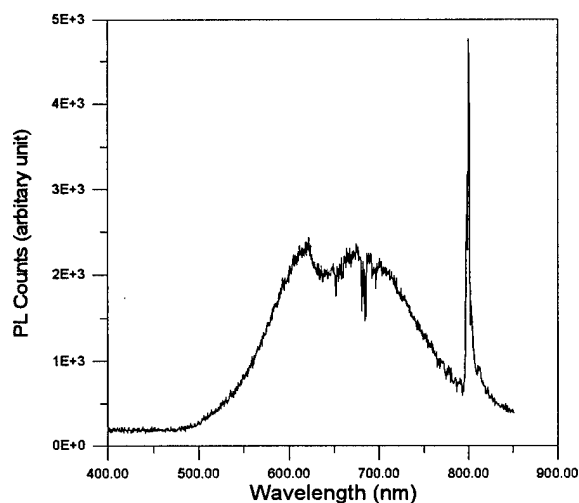
Figure 49



PL of ZnO:Er with Li at T=300K,
exec@514.5nm, 200mW

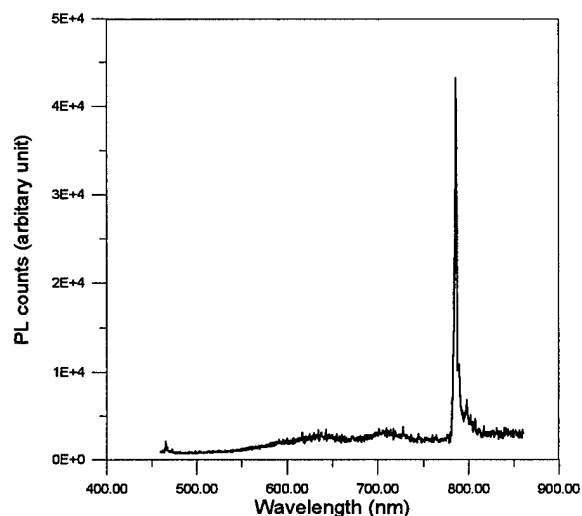
Figure 50

Figure 47-50: shows the PL spectra of ZnO: Er, Li excited by Ar^+ laser line at 457.9 nm, (200 mW) recorded at 10, 100, 200 and 300 K. The spectra on Fig. 50 shows Er^{3+} emission at 300K, the peaks at ~ 538 nm assigned to transition $^4\text{H}_{11/2} \rightarrow ^4\text{I}_{15/2}$, the dominant peaks at 555 nm assigned to transition $^4\text{S}_{3/2} \rightarrow ^4\text{I}_{15/2}$, peaks at 660 nm ($^4\text{F}_{9/2} \rightarrow ^4\text{I}_{15/2}$), a wide band at ~ 750 nm ($^4\text{I}_{9/2} \rightarrow ^4\text{I}_{15/2}$), and peaks at 862 nm ($^4\text{S}_{3/2} \rightarrow ^4\text{I}_{13/2}$).



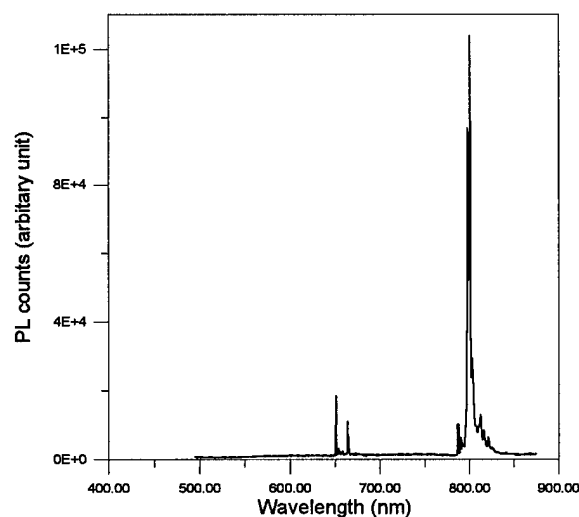
PL intensity of ZnO:Tm
(exc laser @325nm Temp 100K)

Figure 51



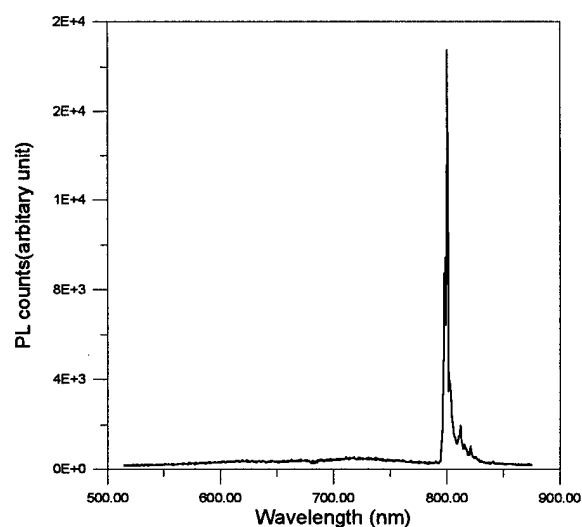
PL of ZnO:Tm with Li at T=9K
exc @ 457.9 nm, 50mW

Figure 52



PL of ZnO:Tm with Li at 9K
exc @ 476nm, 50mW

Figure 53



PL of ZnO:Tm with Li at 9K
exc @ 496.5nm, 50mW

Figure 54

Figure 51-54 shows the PL spectra of ZnO: Tm, Li excited by He-Cd laser (325nm, 30 mW), and Ar⁺ laser line at 457.9 nm, 476 nm, and 496.5 nm (50 mW) recorded at 100K (Fig.51), and 9 K (Fig. 52-54). The spectra on Fig.53 shows Tm³⁺ emission at 9K, the peaks at ~650 nm correspond to transition $^1G_4 \rightarrow ^3H_4$, the dominant peaks at ~800nm correspond to transition $^1G_4 \rightarrow ^3H_5$, the wide bands with peaks at ~622nm and 675nm on Fig.51 correspond to transition $^1G_4 \rightarrow ^3H_4$.

PL kinetics of ZnO:Dy,Li of Dy 580nm peak at 10K
exec.@457.9nm, 80mW

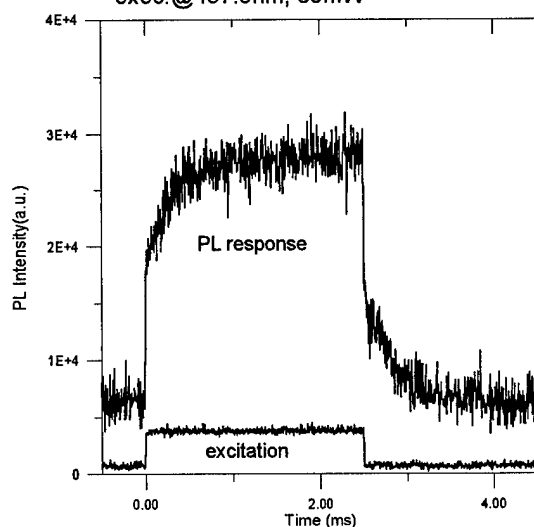


Figure 55

PL kinetics of ZnO:Dy,Li of Dy 580nm peak at 10K
exec.@476.5nm, 80mW

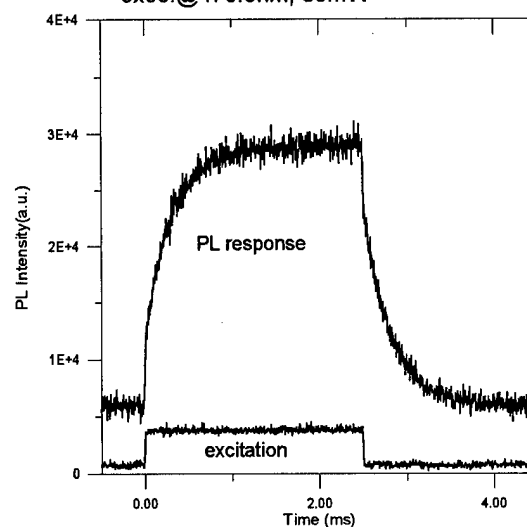


Figure 56

PL kinetics of ZnO:Er,Li of Er 560nm peak at 10K
exec.@488.0nm, 80mW

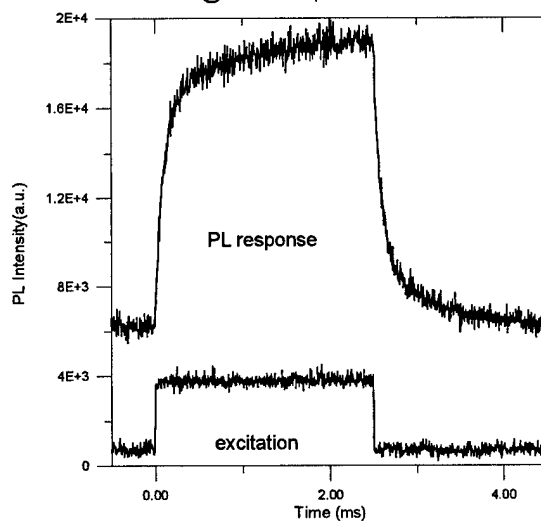


Figure 57

PL kinetics of ZnO:Er,Li of Er 560nm peak at 10K
exec.@514.5nm, 80mW

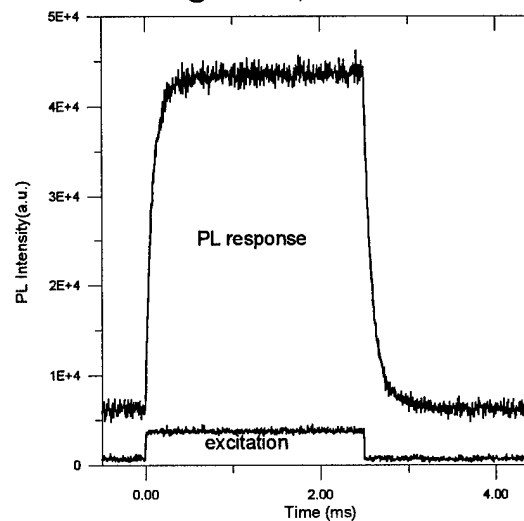


Figure 58

Figures 55, 56 PL rise and decay kinetics of transition ${}^4F_{9/2} \rightarrow {}^6H_{13/2}$ for ZnO: Dy,Li excited at two different wavelengths 457.9 nm and 476.5nm with power 80 mW. Figures 57,58, show the PL rise and decay kinetics of ${}^4H_{11/2} \rightarrow {}^4I_{15/2}$ transition for ZnO: Er,Li excited at two different wavelength 488 nm and 514.5 nm respectively with power 80 mW. Figures 55-58 shows also the excitation laser pulses.

Table IV

Double Exponential Curve Fitting for Rise and Decay Time					
Figure Number	Rise Time of Fast Process	Rise Time of Slow Process	Decay Time of Fast Process	Decay Time of Slow Process	Descriptions of transitions
1	11 μ s	329 μ s	5.4 μ s	436 μ s	ZnO:Dy,Li;580nm $^4F_{9/2} \rightarrow ^6H_{13/2}$
2	7.7 μ s	305 μ s	4.4 μ s	306 μ s	ZnO:Dy,Li;580nm $^4F_{9/2} \rightarrow ^6H_{13/2}$
3	95 μ s	882 μ s	85 μ s	627 μ s	ZnO:Er,Li;556nm $^4H_{11/2} \rightarrow ^4I_{15/2}$
4	76 μ s	265 μ s	79 μ s	270 μ s	ZnO:Er,Li;556nm $^4H_{11/2} \rightarrow ^4I_{15/2}$

Investigations of PL at different temperature, excitation spectra, time resolved spectra, and photoluminescence kinetics are in progress. The results of the described investigation will be published and presented at meetings in the near future. The below Tables IV show the preparation details of single crystals, microcrystalline powders GaN, ZnO, and sintered pellets of GaN, ZnO. The concentration of rare earth, of codopants, the chemical compounds used, the firing temperature, duration time, and ambient atmosphere.

References

1. R.B. Zetterstrom, J. Of Materials Science 5, 1102,(1970)
2. A. Rabenau, in "Compound Semiconductors", edited by R.K. Willardson and H.L. Goering, (Academic Press; New York, 1961) Ch. 19, Vol I.
3. T. Ogino and M. Aoki, Jap. J. Of Appl. Phys. 19, 2395,(1980).

TABLE V**Synthesis and growth of single crystals of GaN**

Samples	Annealing Conditions
Ga ₂ O ₃	72 hrs at 1170 ⁰ C in NH ₃
Ga ₂ O ₃ + 1.3%Dy ₂ O ₃	3 hrs at 1150 ⁰ C in NH ₃

Synthesis of Microcrystalline GaN

Samples	Annealing Conditions
Ga ₂ O ₃	3hrs at 1135 ⁰ C in NH ₃
Ga ₂ O ₃	3 hrs at 800 ⁰ C in NH ₃
Ga ₂ O ₃ +0.1%Er(NO ₃) ₃ .5H ₂ O (0.04%Er)	3hrs at 1135 ⁰ C in NH ₃
Ga ₂ O ₃ +0.1%Er(NO ₃) ₃ .5H ₂ O, (0.04%Er)	8 hrs at 1135 ⁰ C in NH ₃
Ga ₂ O ₃ +3.2%Er(NO ₃) ₃ .5H ₂ O (1.2%Er)	8 hrs at 1135 ⁰ C in NH ₃
Ga ₂ O ₃ +2.6%Er(NO ₃) ₃ .5H ₂ O +3.4%Li ₂ CO ₃ (0.96%Er)	8 hrs at 1135 ⁰ C in NH ₃

=====

GaN	3 hrs at 1100 ⁰ C in NH ₃
GaN+0.6%TbF ₃ (0.44%Tb)	3 hrs at 1100 ⁰ C in NH ₃
GaN+1.2%TbF ₃ (0.88%Tb)	2.5 hrs at 1100 ⁰ C in NH ₃
GaN+0.76%TmF ₃ (0.57%Tm)	3 hrs at 1100 ⁰ C in NH ₃
GaN+1.36%NdF ₃ +0.12%Li ₃ N, (0.97%Nd)	3 hrs at 1100 ⁰ C in NH ₃
GaN+0.004%Tb ₄ O ₇ +1%NaCl, (0.0034%Tb)	3.5 hrs at 1100 ⁰ C in NH ₃
GaN+0.254%Tb ₄ O ₇ , (0.22%Tb)	3 hrs at 1100 ⁰ C in NH ₃

Pellets:

GaN+3.8%Er ₂ O ₃ , (3.3%Er)	2hrs at 1000 ⁰ C, in N ₂ , and 1 hr at 1100 ⁰ C in NH ₃
GaN+2.9%Er(NO ₃) ₃ .5H ₂ O, (1.1%Er)	2hrs at 1000 ⁰ C, in N ₂ , and 1 hr at 1100 ⁰ C in NH ₃
GaN+3.9%Er ₂ O ₃ +2.6%Li ₂ CO ₃ , (3.4%Er)	3hrs at 1100 ⁰ C in NH ₃
GaN+3.0%Er(NO ₃) ₃ .5H ₂ O+ +2.9%Li ₂ CO ₃ , (1.1%Er)	3hrs at 1000 ⁰ C in air

Synthesis of Microcrystalline ZnO doped with rare earth.

ZnO+1.3%Dy₂O₃+2.6%Li₂CO₃, 0.6%Dy, 5.75%Li, 5hrs at 1100⁰ C in air

ZnO+4.3%Nd(NO₃)₃·6H₂O + 3.6%Li₂CO₃ 5hrs at 1000⁰ C in air

ZnO+4.5%Tm(NO₃)₃·6H₂O + 3.6%Li₂CO₃ 5hrs at 1000⁰ C in air

=====

ZnO+3.0%Er₂O₃ (2.6%Er) 5hrs at 1000⁰ C in air

ZnO+0.9%Er₂O₃ (0.78%Er) 5hrs at 1000⁰ C in air

ZnO+0.7%Er₂O₃ (0.61%Er) 5hrs at 1000⁰ C in air

ZnO+0.5%Er₂O₃ (0.44%Er) 5hrs at 1000⁰ C in air

=====

ZnO+3.0%Er(NO₃)₃·5H₂O, (1.1%Er) 5 hrs at 1000⁰ C in air

ZnO+3.0%Er(NO₃)₃·5H₂O+

+2.5%Li₂CO₃, (1.1%Er, 0.25%Li) 5hrs at 1000⁰ C in air

ZnO+5.0%Li₂CO₃ 5hrs at 1000⁰ C in air

ZnO+3.0%Er(NO₃)₃·5H₂O+

+4.8%Li₂CO₃, (1.1%Er, 0.5%Li) 5hrs at 1000⁰ C in air

1. U. Saha, and H. J. Lozykowski,

“Photoluminescence Kinetics Model of P-type GaAs: Nd.”

**MATERIALS RESEARCH SOCIETY
SYMPOSIUM PROCEEDINGS VOLUME 422**

Rare Earth Doped Semiconductors II

Symposium held April 8-10, 1996, San Francisco, California, U.S.A

EDITORS:

Salvatore Coffa

*CNR-IMETEM
Catania, Italy*

Albert Polman

*FOM-Institute AMOLF
Amsterdam, The Netherlands*

Robert N. Schwartz

*Hughes Research Laboratories
Malibu, California, U.S.A.*



PITTSBURGH, PENNSYLVANIA

PHOTOLUMINESCENCE KINETICS MODEL OF P-TYPE GaAs:Nd

U. K. Saha, and H. J. Lozykowski, , School of Electrical Engineering and Computer Science, Ohio University, Athens, Ohio 45701

ABSTRACT

In this work we have developed a model for the kinetics of the energy transfer from the host lattice to the core states of rare earth (RE) centers. We have derived a set of kinetics differential equations of RE luminescence in p-type semiconductor. Numerically computed rise and decay time of RE luminescence as a function of excitation power shows good agreement with the experimental data obtained for p-type GaAs:Nd.

INTRODUCTION

Rare earth (RE) doped III-V semiconductors are very attractive for new light emitting device applications such as lasers and LEDs. In this case emission is no more Band to Band recombination but on the internal emission of the RE^{3+} ions. Among the rare earth doped in III-V semiconductors InP:Yb has been the most extensively studied. It was found that Ytterbium in InP replaces indium on a substitutional site and creates an isoelectronic electron trap at 30 meV below the conduction band (CB). For the case of Nd in GaAs, Takahei [1] proposed similar trap level ranging 80 - 120 meV exists below the CB. Nd in III-V semiconductor is of particular interest due to its four-level laser scheme. In this article, we have developed photoluminescence (PL) kinetics model for p-type III-V semiconductors doped with RE^{3+} ions, where RE^{3+} replaces the element from column III. A numerical approach was encountered to solve the rise and decay of the luminescence of the developed kinetic model for p-type GaAs:Nd. Study of the rise time at different excitation intensities and pulse duration, and temperatures can provide important information about the energy transfer and recombination (radiative and non-radiative) processes.

EXPERIMENTAL SETUP

The experimental data used in this paper were obtained at NTT Basic Research Laboratory in Tokyo [2]. Nd-doped GaAs epitaxial layers were grown by low-pressure metal organic chemical vapor deposition (MOCVD). The p-type GaAs:Nd with the hole concentration $1.4 \times 10^{14} \text{ cm}^{-3}$ at room temperature was investigated in this study. The PL measurements were carried out using an argon-ion laser (Ar^+) operating at 514.5 nm. The pulse excitation for kinetic measurements was obtained by acousto-optic light modulator (model A140 CS). The detecting electronics consisted of Hamamatsu R632-1S photo multiplier. The signals from the photo multiplier was fitted through to the photon counters SR 430 to measure the PL rise and decay kinetics. Different excitation intensities were used to see the variation of rise and decay time. The complete PL spectrum of Nd-doped GaAs is shown in figure 1a. These emission lines correspond to the Nd^{3+} ion intra-4f-shell transitions $^4F_{3/2} \rightarrow ^4I_{13/2}$ at 0.9 eV, $^4F_{3/2} \rightarrow ^4I_{11/2}$ at 1.1 eV, and $^4F_{3/2} \rightarrow ^4I_{9/2}$ at 1.346 eV respectively. Figure 1b shows PL emission lines peaking at 921.0 nm (1.346 eV) which are attributed to the transition $^4F_{3/2} \rightarrow ^4I_{9/2}$ of the Nd^{3+} ion. The PL rise and decay kinetics of Nd^{3+} transition $^4F_{3/2} \rightarrow ^4I_{9/2}$ at 921 nm as a function of excitation intensity was investigated for p-type GaAs doped with neodymium.

This wavelength was chosen since the photocounting system with photomultiplier had the long wavelength limit at about 1100 nm.

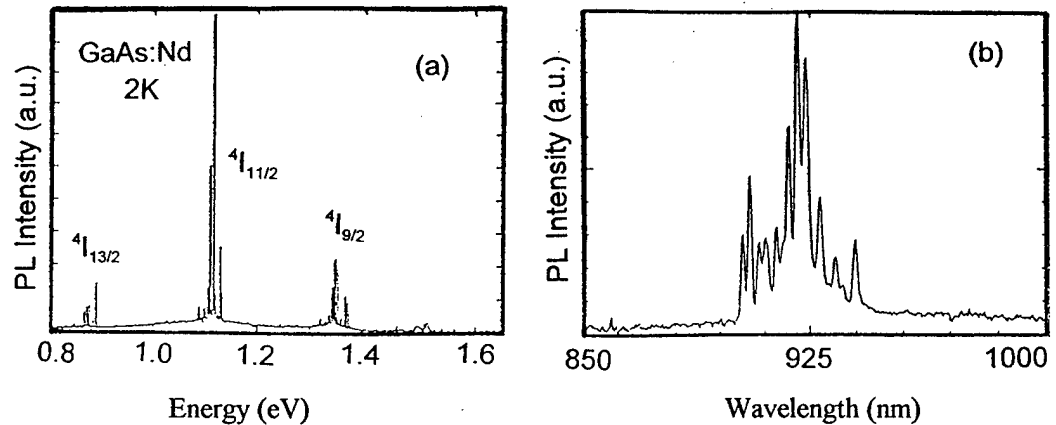


Fig. 1: PL spectra of p-type GaAs:Nd. (a) complete emission spectrum of Nd³⁺ in GaAs [3], and (b) emission spectra attributed to transition ${}^4F_{3/2} \rightarrow {}^4I_{9/2}$ peaked at 921.0 nm.

KINETIC MODEL AND COMPUTATION RESULTS

The RE structured isoelectronic centers can exist in six possible states. These are (1) neutral unoccupied trap (concentration N_0), (2) neutral excited trap (concentration N_o^*), (3) exciton occupied trap (concentration N_x), (4) negatively charged trap (concentration N_-), (5) excited negatively charged trap (concentration N_-^*), and (6) excited exciton occupied trap (concentration N_x^*). The RE luminescence is due to the radiative transitions between $4f^n$ core states of the RE element. Total intensity of the RE emission is the sum of the radiative transition of N_o^* , N_-^* , and N_x^* to N_0 , N_- , and N_x respectively. The radiative recombination of excited RE³⁺ ions in crystals occurs predominantly by magnetic and electric dipole transitions [4]. Electric-dipole transitions between $4f^n$ levels are strictly parity forbidden (Laporte's selection rule). The parity prohibition can be lifted by the influence of the crystal lattice. If the RE ion is located at a site that is a center of symmetry in the crystal lattice the parity prohibition cannot be lifted and only magnetic-dipole transitions are allowed. For RE ions residing in a lattice site lacking inversion symmetry like semiconductors with T_d symmetry, the parity prohibition can be canceled by mixing the $4f^n$ configuration with a state possessing a different parity. Typically the lifetime of the magnetic-dipole transition is $10^4 - 10^5$ times longer than the lifetime of a level that recombines via an allowed electric-dipole transitions. In InP:Yb and GaAs:Nd semiconductors the radiative lifetime at low temperature is in the range of 12 μ s and is probably dominated by electric-dipole transition.

In our model we will assume that isoelectronic trap is an electron trap such as Yb³⁺ in InP. With the intrinsic excitation the electron from the valence band will go to CB and may fall into the isoelectronic trap and create N. (Fig. 2a). From this stage two important energy transfer processes may occur to core state of REI impurities. First, the N. center can be transformed to the N_o^* center through an Auger process where the recombination energy of the bound electron with free hole is transferred non-radiatively to the core states with a rate, $r_T = B_T N. p$, where B_T is the energy transfer coefficient, and p is the free hole concentration.

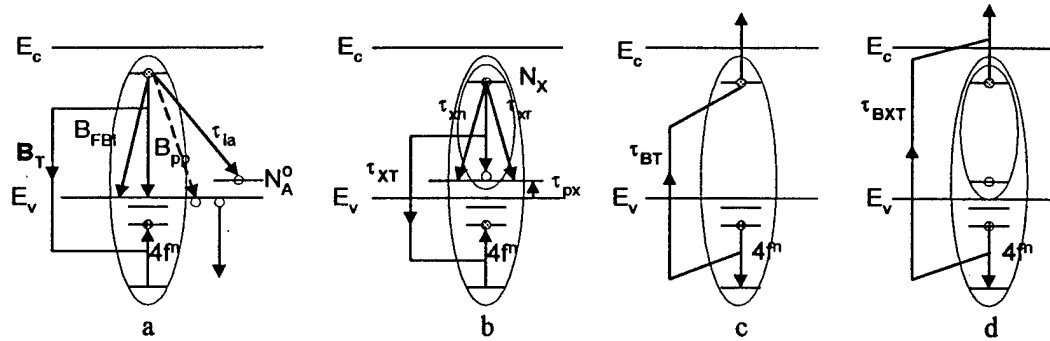


Fig. 2. Auger energy transfer processes to core states (a) from the annihilation energy of the bound electron to free hole, (b) from the bound exciton on a REI trap. Energy back transfer processes: (c) from the excited core states to bound electron on the trap, and (d) from the excited REI-trap to bound exciton.

Second, electron on the trap can attract a hole from valance band with time τ_{px} and create a bound exciton (N_X) (Fig. 2b). The striking feature of this bound exciton is a long luminescence decay time, ranging from few hundred to few thousand nanoseconds [5]. For example, the lifetime of an exciton bound to a Bi isoelectronic trap in InP is about 200 ns [5]. Energy of that bound exciton on a REI trap may transfer non-radiatively via Auger process to core states with the rate $r_{XT} = B_{XT} N_X$, where B_{XT} is the transfer coefficient, and τ_{XT} is the characteristics time. The radiative recombination of the bound exciton on REI trap has long lifetime compare to the energy transfer time τ_{XT} . That's why we do not observe the luminescence of excitons bound to REI trap. The bound exciton to isoelectronic trap N_X can thermally dissociate by either of two processes: (1) it can dissociate into a free exciton (X) and neutral N_0 and (2) it can dissociate with the liberation of a hole or an electron with time τ_{xp} or τ_{et} respectively. If the initial and final states are not resonant, the energy mismatch must be accommodated in some way such as phonon emission or absorption.

The N_0 may also recombine radiatively or non-radiatively (via the Auger process) with a hole in the valence band with transition rate $r_{FBI} = B_{FBI} (N_0 \text{ or } N_0^*) p$ and $r_{PP} = B_{PP} (N_0 \text{ or } N_0^*) p^2$, respectively (Fig. 2a), or recombine radiatively with a hole trapped on a distant acceptor. These three processes transform the N_0 center into the N_0^0 neutral trap. The exciton bound to N_X can thermally dissociate by several processes. It can dissociate a free exciton and neutral trap (N_0) or it can dissociate with liberation of hole or electron with time τ_{xd} . The result of the two energy transfer processes to core states defined by B_T and r_{XT} leads neutral excited trap (N_0^*). If the lifetime of the N_0^* is long, an electron can be captured into that trap and transformed into an N_-^* center. The N_-^* may lose the electron through processes described above (Fig. 2a), or by an auto-deionization Auger process ($N_-^* \rightarrow N_0 + e_{kinetic}$) with characteristic time τ_{BT} described in figure 2c. This process is called Auger back transfer process. Electron trapped on N_-^* can also create an excited bound exciton, N_X^* and it may be dissociated with the liberation of hole or electron with characteristic time τ_{BXT} by the de-excitation energy transition between $4f^n$ core states (Fig. 2d) and become N_0 . Exciton bound to excited REI trap, N_X^* , can thermally dissociate into free exciton and becomes N_0^* .

Figure 3a shows an example of non-radiative recombination involving the interaction of a N_0^* with an electron trapped on N_0 and an electron trapped on a N_-^* . The de-excitation

energy of N_o^* may be transferred non-radiatively via Auger process creating "hot" hole in the valence band by ejecting electron from the valence band to acceptor level (Fig. 3b) or to a hole by ejecting it into the deep valence band (Fig. 3c). Wang and Wessels [6] reported that free carrier Auger processes play a limited role in determining the Er^{+3} luminescence efficiency in InP crystal. This is because probability of formation of bound excitons at the rare earth centers increases with the increase of free carrier concentration from 10^{13} to 10^{17} . Considering this situation in our model we have ignored the free carrier Auger processes.

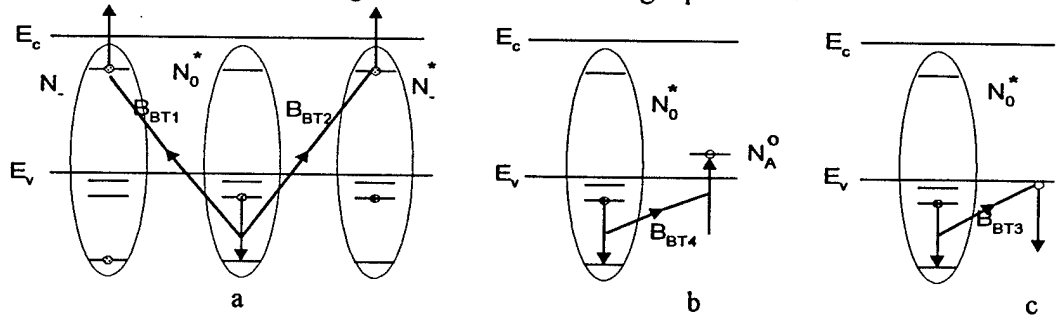


Fig. 3: Auger nonradiative recombination involving the interaction of the core excited REI-trap (N_o^*) with (a) an electron trapped on separate centers N_- and N_+ , (b) an electron in the valence band, and (c) a hole in the valence band.

The excited RE ion may decay by radiating, by a cross relaxation process (which is not important at low RE concentration used), or by the multiple emission of phonons. Investigations in different host materials [5] show that nonradiative recombination involving the generation of more than five phonons is weaker than the radiative process. Nonradiative recombination for Er and Nd in GaAs and Yb in InP would require the generation of 21, 36 and 27 LO phonons, respectively. In GaAs oxygen related centers produced the IR absorption bands centered at 845 cm^{-1} (104.7 meV) and 715 cm^{-1} (88.6 meV) due to localized vibrational modes (LVM) [7]. Oxygen atoms due to ability of forming strong bonds create impurities complexes and show IR absorption spectra. Oxygen can also create complexes with rare earth ions [8]. The very high energy optical phonons derive from internal vibrational modes of the oxygen complexes, may interact with the RE ions differently from the low-energy lattice LO phonons [9]. The quenching process involving vibration modes required additional study planned for the near future. Energy migration due to the quenching center can also play an important role in the quenching of RE luminescence at high temperature.

According to above discussion we have developed the kinetic equations (3) to (13). To solve this system we have assumed the band gap excitations take place at low temperature (in our experiment 2 K) so that thermal activation of the trapped carriers is negligible. That is, terms explicitly dependent on temperature were ignored, and only trapping, transferring, and recombination transitions were considered. The numerical solution was obtained using the fitting parameters stated in table 1. The experimental and numerically simulated luminescence rise and decay are shown in figure 4 at different excitation intensities. All profiles are normalized to unity at maximum. The rise and decay time of the dominant component of the double exponential fitting are shown in table 2. From table 1 we see that Auger energy transfer coefficient of bound electron to free hole (B_T) is $3 \times 10^{-5}\text{ cm}^3$ per sec. But for semi-insulating (SI) InP:Yb, B_T was equal to $4 \times 10^{-10}\text{ cm}^3$ per second [5], which indicates that

$$\frac{dN_-}{dt} = \frac{n}{\tau_{et}} \left(\frac{N_0}{N} \right) + \frac{N_-^*}{\tau_3} + \frac{1}{\tau_{px}} \left(\frac{N_x}{N} \right) \frac{N_v}{\beta_h} \exp\left(-\frac{E_h}{kT}\right) - \frac{1}{\tau_{et}} \left(\frac{N_-}{N} \right) \beta_i N_c \exp\left(-\frac{E_i}{kT}\right) - \frac{p}{\tau_{px}} \left(\frac{N_-}{N} \right) - B_{FBI}(N_-) p - B_{BT1} N_0^* (N_-) - B_T(N_-) p \quad (3)$$

$$\frac{dN_x}{dt} = \frac{N_x^*}{\tau_3} + \frac{p}{\tau_{px}} \left(\frac{N_-}{N} \right) - N_x \left(\frac{1}{\tau_2} + \frac{1}{\tau_{xT}} + \frac{1}{\tau_{xd}} \right) - \frac{1}{\tau_{px}} \left(\frac{N_x}{N} \right) \frac{N_v}{\beta_h} \exp\left(-\frac{E_h}{kT}\right) \quad (4)$$

$$\frac{dN_0^*}{dt} = \frac{N_x}{\tau_{xT}} + B_T(N_-) p + \frac{1}{\tau_{et}} \left(\frac{N_-^*}{N} \right) \beta_i N_c \exp\left(-\frac{E_i}{kT}\right) - \frac{n}{\tau_{et}} \left(\frac{N_0^*}{N} \right) - \frac{N_0^*}{\tau_3} - B_{BT1}(N_-) (N_0^*) - B_{BT4}(N_0^*) (N_0^*) \quad (5)$$

$$\frac{dN_-^*}{dt} = \frac{n}{\tau_{et}} \left(\frac{N_0^*}{N} \right) + \frac{1}{\tau_{px}} \left(\frac{N_x}{N} \right) \frac{N_v}{\beta_h} \exp\left(-\frac{E_h}{kT}\right) - N_-^* \left(\frac{1}{\tau_3} + \frac{1}{\tau_{BT}} \right) - B_{FBI}(N_-^*) p - \frac{p}{\tau_{px}} \left(\frac{N_-^*}{N} \right) - \frac{1}{\tau_{et}} \left(\frac{N_-^*}{N} \right) \beta_i N_c \exp\left(-\frac{E_i}{kT}\right) - B_{BT2} N_0^* (N_-^*) \quad (6)$$

$$\frac{dN_x^*}{dt} = \frac{p}{\tau_{px}} \left(\frac{N_-}{N} \right) - N_x^* \left(\frac{1}{\tau_2} + \frac{1}{\tau_3} + \frac{1}{\tau_{xd}} + \frac{1}{\tau_{BXT}} \right) - \frac{1}{\tau_{px}} \left(\frac{N_x^*}{N} \right) \frac{N_v}{\beta_h} \exp\left(-\frac{E_h}{kT}\right) \quad (7)$$

$$\frac{dn}{dt} = G + N_x^* \left(\frac{1}{\tau_{xd}} + \frac{1}{\tau_{BXT}} \right) + \left(\frac{N_- + N_-^*}{N} \right) \frac{1}{\tau_{et}} \beta_i N_c \exp\left(-\frac{E_i}{kT}\right) + \frac{N_x}{\tau_{xd}} + \frac{N_-^*}{\tau_{BT}} - \frac{n}{\tau_{et}} \left(\frac{N_0 + N_0^*}{N} \right) + B_{BT1} N_0^* (N_-) + B_{BT2} (N_0^*) N_-^* \quad (8)$$

$$\frac{dp}{dt} = G + \frac{\beta_A}{\tau_{px}} \left(\frac{N_x}{N} + \frac{N_x^*}{N} \right) - \frac{p}{\tau_{px}} \left(\frac{N_-}{N} + \frac{N_-^*}{N} \right) - B_{FBI}(N_- + N_-^*) p + B_{BT4} N_0^* N_A^0 - \left(1 - \frac{N_A^0}{N_A} \right) \frac{p}{\tau_{pA}} + \left(\frac{N_A^0}{N_A} \right) \left(\frac{1}{\beta_A} \right) \frac{N_v}{\tau_{pA}} \exp\left(-\frac{E_A}{kT}\right) \quad (9)$$

$$\frac{dN_A^0}{dt} = \left(1 - \frac{N_A^0}{N_A} \right) \frac{p}{\tau_{pA}} - \left(\frac{N_A^0}{N_A} \right) \left(\frac{1}{\beta_A} \right) \frac{N_v}{\tau_{pA}} \exp\left(-\frac{E_A}{kT}\right) - B_{BT4} N_0^* N_A^0 \quad (10)$$

$$N = N_0 + N_- + N_x + N_0^* + N_-^* + N_x^* \quad (11)$$

$$N_A = N_A^0 + N_A^- \quad (12)$$

$$p = n + N_- + N_-^* - \left(1 - \frac{N_A^0}{N_A} \right) N_A \quad (13)$$

Table 1: Parameters describing Rise and Decay kinetics of GaAs:Nd

Symbol	Unit	Parameter value
τ_3	second	11.7×10^{-6}
τ_{BT}	second	500×10^{-9}
τ_{XT}	second	1×10^{-9}
τ_{BXT}	second	9×10^{-6}
τ_{et}	second	1×10^{-8}
τ_{px}	second	4.91×10^{-12}
τ_{xd}	second	1×10^{-12}
τ_{pA}	second	500×10^{-9}
B_T	$\text{cm}^3/\text{second}$	3×10^{-5}
B_{FBI}	$\text{cm}^3/\text{second}$	1×10^{-15}
B_{BT1}	$\text{cm}^3/\text{second}$	1×10^{-14}
B_{BT2}	$\text{cm}^3/\text{second}$	1×10^{-14}
B_{BT4}	$\text{cm}^3/\text{second}$	4×10^{-18}

transfer rate of the annihilation energy of bound electron to free hole to the core states is faster in p-type GaAs:Nd than in SI InP:Yb. All other parameters used for fitting are in the same range which are used in SI InP:Yb. From table 2 it is easily found that computed rise time is always higher than the experimental rise time. However decay times almost matches with the experimental data. In conclusion the developed PL kinetic model for p-type semiconductor doped with RE gives estimation of the energy transfer process to core states when fitted with the experimental data.

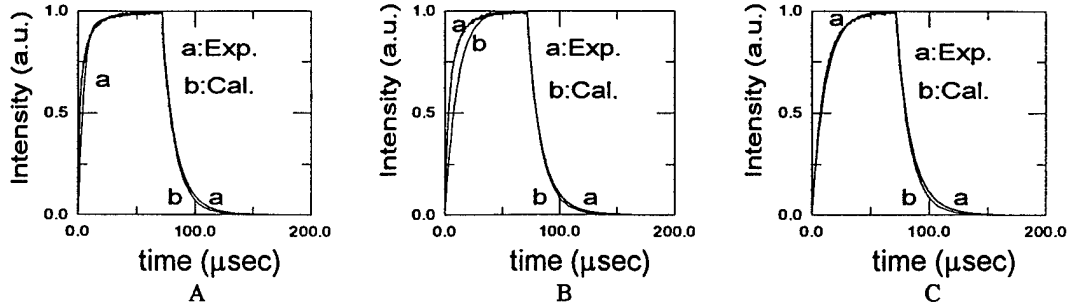


Fig. 4: Experimental (a) and calculated (b) luminescence rise and decay as a function of time, for three excitation intensities, A) 18 mW, B) 2.24 mW, and C) 0.24 mW. Pulse width is 71.4 μ sec.

Table 2: Theoretical and experimental rise and decay times as a function of power.

Excitation power	Rise time (μ sec.)		Decay time (μ sec.)	
	Experimental	Theoretical	Experimental	Theoretical
18 mW	1.91	3.1	9.421	9.421
2.243 mW	5.4	9	10.5	11.2
0.24 mW	9	10	13.1	12.52

This work was supported by AFOSR grant No. F49620-1-0024, Ohio University CMSS Program, and Ohio University SEECs Stocker Fund.

REFERENCES

1. M. Taniguchi, H. Nakagome and K. Takahei, Appl. Phys. Lett. **58**, 2930 (1991).
2. H. J. Lozykowski, and K. Takahei, unpublished.
3. H. Nakagome and K. Takahei, Jap. J. Appl. Phys. **28**, 2098 (1989).
4. M. J. Weber, Phys. Rev. Vol. 171, 283 (1968).
5. H. J. Lozykowski, Phys. Rev. **B48**, 17758 (1993), and references cited therein.
6. X. Z. Wang and B. W. Wessels, Appl. Phys. Lett. **65**, 845 (1994).
7. M. Skowronski in, *Deep Centers in Semiconductors* Edited by S.T. Pantelides (Gordon and Breach Science Publishers, Philadelphia, 1992), p.379.
8. H.J. Lozykowski, A. K. Alshawa, and I.Brown, Mat.Res.Soc. Symp. Proc. **417** (1995), in print.
9. E.D. Reed, Jr. And H.W. Moos, Phys. Rev. **B8**, 980 (1973), and references cited therein.

2. H.J. Lozykowski, A. K. Alshawa, and I. Brown,

**“Luminescence Properties of Ytterbium and Oxygen
Coimplanted InP.”**

MATERIALS RESEARCH SOCIETY
SYMPOSIUM PROCEEDINGS VOLUME 417

Optoelectronic Materials: Ordering, Composition Modulation, and Self-Assembled Structures

Symposium held November 28-30, 1995, Boston, Massachusetts, U.S.A.

EDITORS:

Eric D. Jones

*Sandia National Laboratories
Albuquerque, New Mexico, U.S.A.*

Angelo Mascarenhas

*National Renewable Energy Laboratory
Golden, Colorado, U.S.A.*

Pierre Petroff

*University of California, Santa Barbara
Santa Barbara, California, U.S.A.*



PITTSBURGH, PENNSYLVANIA

LUMINESCENCE PROPERTIES OF YTTERBIUM AND OXYGEN COIMPLANTED InP

H.J.Lozykowski, A. K. Alshawa, Ohio University, Athens, Ohio. and I.Brown, Lawrence Berkeley Laboratory, University of California at Berkeley.

ABSTRACT

In this work we report a systematic study of the effect of oxygen on ytterbium 4f-4f emission by coimplanting Yb and O into InP. The PL spectra of InP: Yb and InP: (Yb+O) as a function of annealing temperature and duration were studied. In addition the photoluminescence and kinetic processes were investigated as a function of temperature and excitation intensity. The investigation shows that the codoped oxygen reduces drastically the Yb³⁺ emission from SI and n-type InP:Yb under intrinsic excitation. The codoping of Yb and O may create a complex involving a Yb_{in} and O_p. This structured isoelectronic (Yb_{in} - O_p) complex, may behave as a deep trap (or a deep donor) located approximately at the middle of bandgap. Exciton bound to such centers will not have sufficient energy to excite the core Yb 4f electrons by Auger direct energy transfer process.

INTRODUCTION

There has been increasing interest in rare earth doped semiconductors because of their potential for light emitting device applications. Scientific interest is related to the uniqueness of optical and electrical properties of rare earth impurities in semiconductor hosts. The 4f orbits of rare earth ions incorporated in semiconductors are so deeply buried within the electronic shell that the energy levels of the 4fⁿ configuration are only slightly perturbed as compared to free ion energy levels. Among the rare earth doped III-V semiconductors InP:Yb is the most extensively studied [1,2]. Ytterbium in InP replaces indium on a substitutional site and acts as an isoelectronic trap.

The emission is the result of the internal 4f-4f transitions between crystal field split ²F_{5/2} and ²F_{7/2} levels in Yb³⁺ ion. The Yb³⁺ spectrum in InP arises from the cubic Yb³⁺-center, which most likely is located on a substitutional cation site. Beside this dominant cubic (T_d) center, a Yb³⁺ center with trigonal symmetry was also identified [1,2].

In this work, we report a systematic study of the effect of oxygen on ytterbium 4f-4f emission by coimplanting Yb and O into InP. The PL spectra of InP: Yb and InP: (Yb+O) as a function of annealing temperature and duration were studied. The photoluminescence and kinetic processes were also investigated as a function of temperature and excitation intensity.

RARE EARTH LUMINESCENCE CENTERS IN SEMICONDUCTORS.

The erbium has excited much interest, because the Er³⁺ transition occurs at 1.54 μm, close to the minimum loss region of silica-based optical fibers. In silicon implanted with Er moderate photoluminescence efficiency can be increased by coimplantation of light elements, such as C, N, O, and F, and optimizing the annealing temperature and duration as well as other preparation conditions [3]. It has been concluded from EXAFES study that the optically active center in Czochralski-grown (CZ) silicon is a local sixfold coordinated of oxygen atoms around Er, with the structure similar to that of Er₂O₃ [4]. The same concentration of Er implanted in a high purity float zone (FZ) grown Si crystals which create centers with bonding resembling that of ErSi₂, are

essentially optically inactive. The recent high resolution photoluminescence spectroscopy investigation shows that Er^{3+} created three types of centers in Si [3]: a) isolated, tetrahedral interstitial sites, which is the most stable (the lowest energy configuration for an isolated erbium in Si [5]), b) oxygen-Er complexes with axial symmetry, c) erbium complexes with implantation induced defects. They observe essentially the same spectra for FZ-Si and CZ-Si material although the oxygen content of these crystals do not allow formation of six-fold coordinated Er-O complexes as was claimed in previous paper [4]. The general conclusion from this investigation is that coimplantation Er with light elements does not create Er-codopant complexes, but rather erbium forming complexes with implantation generated lattice defects.

In GaAs and AlGaAs, the erbium characteristic emission was originated from complex involving oxygen as suggested by [6a,b,c]. Cathodoluminescence of GaAs: Er studied under an electron microscope show bright and dark spots. The bright spots as speculated might originate from erbium rich microparticles most probably codoped with oxygen [6c]. Some similar complexes of metal oxygen has already been observed in GaAs doped with Cr and O [6d], and with Be and O [6e]. Colon et al. [7] reports a systematic study of the effect of oxygen on erbium 4f-emission by coimplanting Er and O into GaAs and AlGaAs. They observed very similar increase of PL intensity of Er^{3+} emission from both the $\text{Al}_x\text{Ga}_{1-x}\text{As: Er}$ and $\text{Al}_x\text{Ga}_{1-x}\text{As: (Er+O)}$ with increase Al mole fraction x . The Er^{3+} emission at $1.538 \mu\text{m}$ from $\text{Al}_{0.1}\text{Ga}_{0.9}\text{As: (Er+O)}$ with Er dose of $5 \times 10^{13} \text{ cm}^{-2}$, an O dose of 10^{15} cm^{-2} , and annealed at 750°C increased by one order of magnitude from that of the $\text{Al}_{0.1}\text{Ga}_{0.9}\text{As: Er}$. In contrast similar PL studies on SI GaAs: (Er+O) showed no enhancement rather decreases of the Er^{3+} emissions. In conclusion, authors stated that the efficient luminescence centers are the complex centers: i) associated with not only Er and O, but also with Al, (possibly Er-O-Al complex), or ii) Er-O complex which becomes a very efficient radiative center in a wider bandgap semiconductor. The lack of enhancement, rather decrease of Er emissions from GaAs: (Er+O) samples is explained as follows. Oxygen in an As site, in GaAs is a deep donor 0.75 eV below the conduction band (CB). A complex $\text{Er}_{\text{Ga}} - \text{O}_{\text{As}}$ forming isoelectronic center, may behave as deep donor (or trap) located at about 0.75 eV below conduction band, and remains fixed with respect to the CB edge as x varies. Exciton bound to such center ($\text{Er}_{\text{Ga}} - \text{O}_{\text{As}}$), in GaAs will not have sufficient energy to excite the 4f-4f shell of Er^{3+} . However in $\text{Al}_x\text{Ga}_{1-x}\text{As}$ (for $x \geq 0.1$) with wider bandgap, an exciton bound to an $\text{Er}_{\text{Ga}} - \text{O}_{\text{As}}$ center will have enough energy to excite Er^{3+} . It must be noted that the structures of the emission spectra in investigated samples are changed with annealing temperature (the relative intensity among different peaks). This observation indicated that this emission originated from more than one luminescent center. It is accepted that different Er luminescent centers are formed in III-V semiconductors depending on growing methods and doping techniques. Recently Takahei et al. [8], investigated MOCVD grown GaAs and $\text{Al}_x\text{Ga}_{1-x}\text{As}$ doped with Er and O. The GaAs:(E+O) sample shown only single PL line which splits into more than eight lines by adding 1% of Al to the crystal. Based on the PL spectra, RBS and SIMS analysis they proposed that the structure of erbium luminescent center is $\{\text{Er}_{\text{Ga}} - (\text{O}_{\text{As}})_2\}$, with C_{2v} symmetry. Erbium is occupying the Ga sublattice with two oxygen atoms in the nearest neighbor As sites. The drastic change of emission spectra due to the addition of 1% Al, authors explained by assuming that Al atoms preferentially occupy the nearest neighbor Ga sites of two oxygen atoms, both coupled with Er atom.

The microscopic structure of the Yb^{3+} luminescence center in InP is still not well understood. The SIMS analysis of LPE grown InP: Yb with large amount of Yb shown the homogeneously distributed ytterbium at the level 10^{14} cm^{-3} , the remaining atoms were incorporated as microparticles of Yb compounds, oxides, phosphides and In_3Yb [9a]. Conclusion from Zeeman analysis of PL spectrum of InP:Yb is that spectrum arises from one dominant cubic Yb^{3+}

luminescent center [9b]. The Yb^{3+} ion is residing on an unperturbed T_d indium site [9c]. The existence of only one dominant Yb luminescent center was also confirmed by photoluminescence excitation spectroscopy, and time resolved spectroscopy [1,2,10]. Also the Raman spectra of the InP in the frequency regions of TO phonons (at Γ point) show no crystal lattices distortion when indium atoms were replaced with rare earth ions [2]. Beside the dominant Yb^{3+} cubic center, a Yb^{3+} center with trigonal symmetry ($\text{Yb}^{3+}_{\text{In}} - X_p$) was identified, but the chemical nature of X element is still unknown [1]. The 4f-luminescence of InP: Yb^{3+} is remarkably resistant against fast electron irradiation. An InP: Yb (also in GaP: Yb) sample exposed to 2 MeV electrons beam (fluence of $1 \times 10^{16} \text{ cm}^{-2}$) reduced intensity of the 4f-4f ytterbium emission by a factor of about two, while the near bandgap emission intensity was reduced by more than two order of magnitude [1,11a]. The point defects created by energetic electrons seems to have little influence on Yb^{3+} luminescence. Also no new emission spectra appears from non cubic complex centers formed by association of a Yb^{3+} ion and intrinsic point defects generated by fast electrons. In contrast GaP doped with Nd, Sm, and Eu exposed to 1.6 MeV γ irradiation shows no change of the near bandgap donor acceptor luminescence intensity [11b]. The explanation of this effect is gettering of radiation-induced point defects by rare earth ions. Interesting results were reported on reaction of rare earth with donor and acceptor impurities in GaP, InP and InGaAs [12a,b,c]. For example in GaP, ytterbium actively bonds either oxygen (deep donors) and tellurium. This was monitored by substantial increase in the rate of recombination via donor-acceptor pairs and by disappearance of nitrogen lines and transitions attributed to Zn-O complexes. The rare earth high chemical activity was proposed to utilize for semiconductors purification. It was suggested for the InP crystals grown by the Czochralski method that incorporation of rare earth with smallest radius for example Yb at the cation sites (In), can act for other impurities as a "sinks" where neutral complexes can be formed [2].

Surprisingly, no RE characteristic emission was observed from the semiconductors oxides like ZnO, CdO. Recently for the first time ever we observe strong PL emission of Er and others rare earth at room temperature from ZnO codoped with Li and Er [14]. To best of our knowledge the literatures on the PL of ZnO doped with rare earth, report only the broad almost structure-less emission bands around 550nm, which probably originated from transitions involving same conventional impurities and intrinsic self-activated centers.

SAMPLE PREPARATION AND MEASUREMENTS

Implantation of Yb, was performed with an unconventional implantation technique using a high current metal ion source developed at Berkeley. The InP SI and Sn doped n-type samples were implanted at room temperature at an energy of 150 KeV with Yb, with a dosage of $8 \times 10^{13} \text{ cm}^{-2}$. The co-implantation of oxygen was done with a dose of $1 \times 10^{15} \text{ cm}^{-2}$ at an energy of 22 KeV. The oxygen co-implantation energy was chosen to yield the same projected range as that of Yb to overlap O profile. The simulated depth profile, calculated by Pearson distribution, has the projected range for Yb at 368 Å and O at 405 Å from the surface and a peak concentration $1.7 \times 10^{19} \text{ cm}^{-3}$ and $1.57 \times 10^{20} \text{ cm}^{-3}$, respectively. The rapid thermal annealing system utilizing a strip heater was used to anneal the samples. The RE-implanted InP SI and n-type, samples were annealed at different temperatures, and for different periods of time in forming gas or N_2 (%99.999 pure). In order to provide better protection against surface degradation due to high temperature annealing, the InP samples were placed in a graphite susceptor with reservoirs that are filled with crushed pieces of InP.

The photoluminescence (PL) measurements were carried out using an argon ion laser

operating at 488 nm. The pulsed excitation for rise and decay time measurements was obtained by acousto-optic light modulator. The samples were mounted on a cold finger cooled by a close-cycle helium cryostat down to 8.5K. The emission was dispersed by a Jarrel Ash, 0.75 M, scanning monochromator equipped with a 1180 grooves/mm grating. The detecting electronics consist of thermoelectrically cooled R632-01 photomultiplier with spectral response extended to IR region. The signal from the photomultiplier was fitted through a fast preamplifier to a dual-channel gated photon counting system controlled by a computer, which also controlled the scanning monochromator. The photoluminescence kinetics (rise and decay times) were measured with exceptional accuracy using photon counting system (Turbo-MCS, EG&G Ortec), which offers a wide range of channel dwell times, with no deadtime between channels.

RESULTS AND DISCUSSION

The photoluminescence of Yb-implanted InP was investigated under a CW and pulsed an excitation using Ar⁺ ion laser at different temperatures and excitation intensities. First, the samples were annealed at 660 °C for 10 minutes. The Yb emission spectra of InP: Yb (SI and n-type) consist of a sharp peak at 1001 nm and two broader peaks at 1005.5 nm and 1007 nm (transitions $^2F_{5/2} - ^2F_{7/2}$). In the case of the SI InP:Yb sample, the PL spectra consist only of a strong Yb³⁺ emission with no near-bandgap emission. After the coimplantation of O, the Yb³⁺ emission was weakened and the near-bandgap emission at 897.6 nm (1.38 eV) appeared. For the n-type sample, the emission spectra of InP:Yb consist of the Yb³⁺ emission and a weaker broad bands emission. The coimplantation of O caused a three times increase of the band emission intensity (as compared to InP:Yb) while the Yb³⁺ emission almost disappeared.

In order to study the effect of annealing conditions, the InP:Yb and InP:(Yb+O), both SI samples were annealed at different temperatures and time periods. The Yb and oxygen co-implanted SI-InP samples were annealed at 660 °C for 0.5, 3, 10 and 15 minutes. For the InP:Yb+O samples, annealed at 660 °C for 30 seconds and 15 minutes, the PL emission spectra consisted only of the near-bandgap emission at 897.6 nm (1.38 eV) and no emission due to Yb³⁺ was observed. In the case of the samples annealed for 3 and 10 minutes at 660 °C, both, Yb³⁺ and near-bandgap emission is observed.

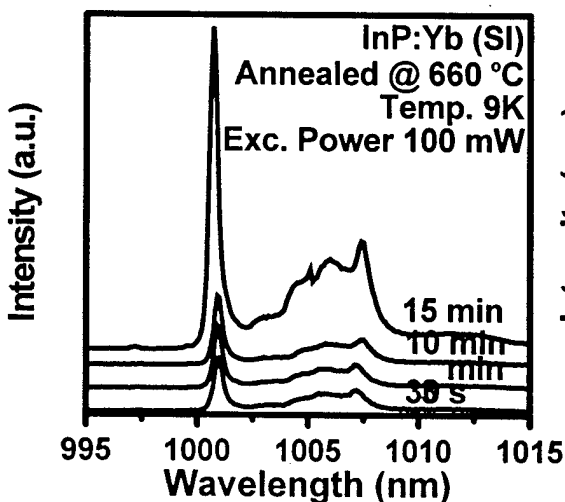


Fig. 1 PL Spectra of InP:Yb (SI) annealed at 660 °C for different time periods.

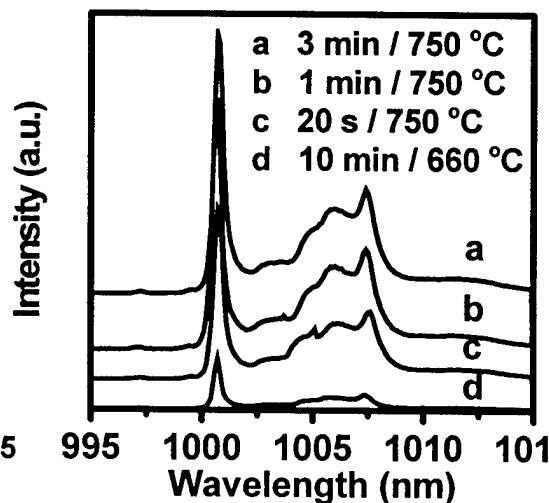


Fig. 2 PL spectra of InP:Yb (SI) annealed at different temperatures and time periods

We carried out similar PL studies on the SI and n-type samples of InP:Yb, and InP:(Yb+O) (implanted at energy and doses as mentioned above) but annealed at 660 °C and 750 °C for various time durations as shown in Fig. 1, 2 and 3. The Yb³⁺ emission intensity observed from SI-InP: Yb annealed at 750 °C during 3 minutes is about 13 times stronger from that of the SI-InP: Yb annealed at 660 °C, during 3 minutes, and 2.27 times stronger from a sample annealed at 660 °C, during 15 minutes. The PL intensity of the Yb³⁺ emission from SI-InP: Yb annealed at 750 °C during 5 minutes is about 8 times weaker from that of the SI-InP: Yb annealed at 750 °C, during 3 minutes. The PL intensity of the Yb³⁺ emission from SI-InP samples coimplanted with Yb and O annealed at 750 °C during 3 minutes was weaker 28 times (and 106 times weaker from the sample annealed at 660 °C for 10 minutes) from that of the SI-InP: Yb without O annealed at the same conditions.

In general, a very similar PL intensity dependence was observed from Yb and Yb+O doped n-type InP samples, but there are significant differences in PL intensity between them. The PL intensity of the Yb³⁺ emission from n-type InP:Yb is weaker 4.8 times in comparison with SI-InP:Yb samples, both annealed at 750 °C during 3 minutes. The sample of n-type InP:Yb+O, annealed at 750 °C for 3 minutes, shows a 65 time decrease of the Yb³⁺ emission as compared to n-type InP:Yb sample, annealed at the same conditions. The sample n-type InP:(Yb+O) annealed at 660 °C during 3 minutes showed very weak emission, and as annealing time increased to 10 minutes the intensities increased 3.3 times but is still very weak.

The Yb³⁺ emission intensity, the PL rise, and decay time measurements as a function of the excitation power were investigated. The intensity of the Yb 1001 nm emission line as a function of the excitation power in the range of 0.1 - 1600 mW show the emission intensities increase approximately linearly from low power to 1600 mW. The PL kinetic study under square pulse excitation above bandgap shows that the rise and decay times are functions of the excitation power as shown in Fig. 4 [10]. The rise time is determined by the energy transfer processes between the InP host and the Yb³⁺ ions. It is decreasing with increasing excitation power (generation rates). Decay time shows also a decrease but smaller with the increase of a generation rate, and is determined by Auger quenching processes [10].

We also investigated the Yb³⁺ characteristic emission intensity and decay time as a

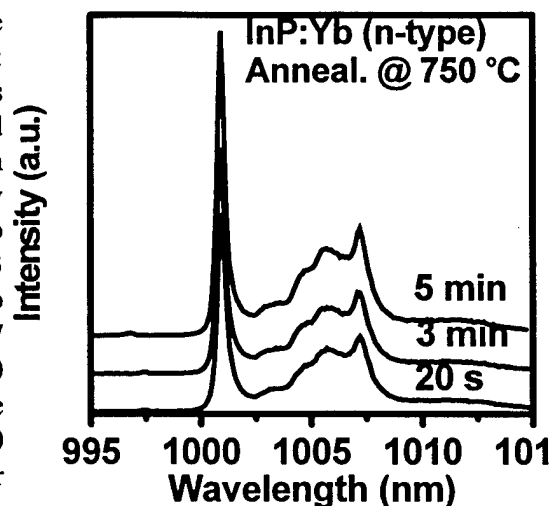


Fig. 3 PL spectra of n-type InP:Yb annealed at 750 °C for different time periods

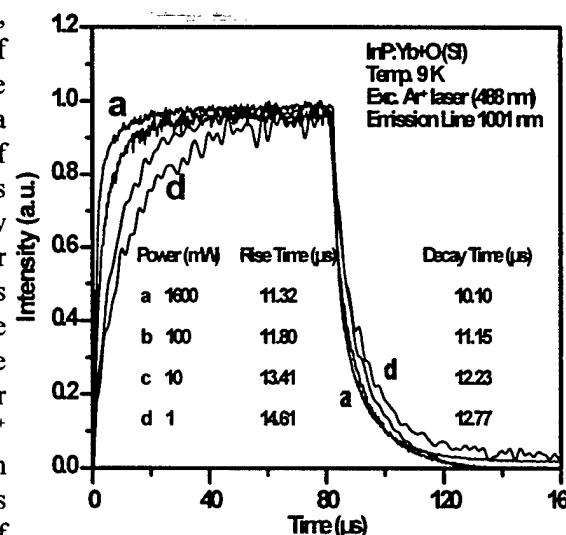


Fig 4 The luminescence rise and decay for different excitation power

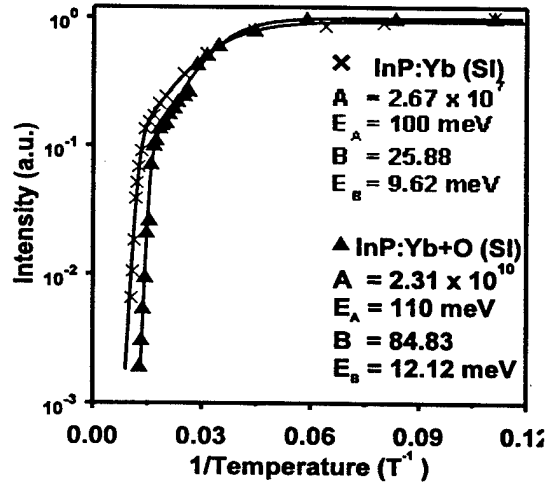


Fig. 5 A fit of the PL intensity versus temperature of InP:Yb and InP:Yb+O, both annealed at 750° C / 3 min

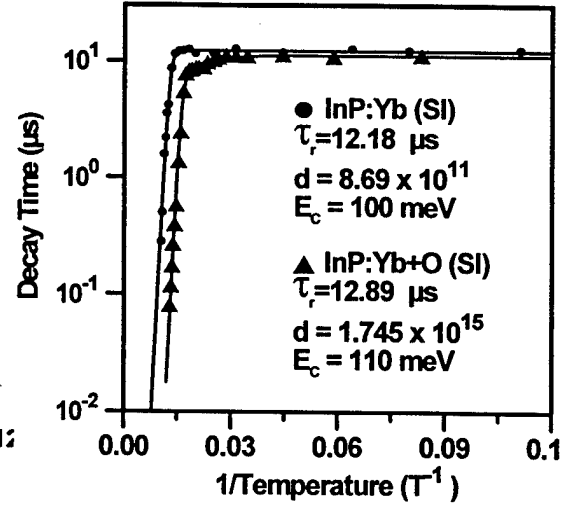


Fig. 6 A fit of the PL decay times versus temperature of InP:Yb and InP:Yb+O, both annealed at 750° C / 3 min

of temperature. The experimental data of the temperature dependence of PL intensity of the 1001 nm emission peak, was fitted to the relationship [10]

$$I(T) = I_0 [1 + A \exp(-E_A/kT) + B \exp(-E_B/kT)]^{-1} \quad (1)$$

The experimental result was plotted with theoretical fitting (solid line) using parameters as shown in Fig. 5. In InP:Yb, the Yb³⁺ PL intensity as a function of temperature remains approximately constant between 8.6 and 80 K, above which it decreases rapidly with further increasing temperature, while in InP:Yb+O, the Yb³⁺ emission intensity remains constant between 8.6 and 60 K. The decay time for the PL of Yb³⁺ as a function of temperature is given by the equation

$$1/\tau = d \exp(-E_c/kT) + 1/\tau_r \quad (2)$$

and the theoretical fitting parameters are shown in Fig. 6. A very similar temperature dependence was observed for the emission intensity and decay time for Yb and Yb+O implanted n-type.

The presented above results show that the addition of oxygen reduces drastically the Yb³⁺ emission from InP:Yb under indirect excitation. Thus, it is very doubtful that the luminescence seen from rare earth doped semiconductors, in our case InP:Yb originates from a complex involving oxygen, as suggested by others (see above). Similar codoping GaAs with both Er and O did not result in any enhancement but rather decrease of Er³⁺ emission [7]. It is established that the excitation of Yb in InP preceeds dominantly through the energy transfer from excitons bound to the RE³⁺ structured isoelectronic traps (REI traps) to the core 4f electrons [12]. The oxygen implantation in InP results in free carrier compensation in both Sn-doped and undoped InP [13a]. Authors observe new traps in an undoped InP after O implantation and rapid thermal annealing at 400° C for 10 seconds located at 0.47 eV and 0.28 eV below the conduction band (CB). The Sn doped InP shows traps at 0.71 eV, 0.37 eV, and 0.15 eV below CB. In GaP oxygen gives a deep donor with activation energy 0.893 eV below the conduction band [13b]. These facts and discussions in the introduction suggested that codoping of Yb and O may create a complex involving a Yb_{in}, Yb in an In site and O_p, oxygen in P sites. This a structured isoelectronic (Yb_{in} - O_p) complex, which may behave as a deep trap (or a deep donor) located approximately

in the middle of bandgap. Exciton bound to such centers will not have sufficient energy to excite the core Yb 4f electron by Auger direct energy transfer process [12]. If proposed model of the complex center is correct, and Yb³⁺ ions are optically active in such centers, the direct excitation of Yb³⁺ 4f electrons by photons, or by direct collision excitation by energetic electrons, should not show quenching of Yb³⁺ characteristic (²F_{5/2} - ²F_{7/2}) emission. The direct excitation of Yb³⁺ ions by photons, using Ti-sapphire laser, electroluminescence and cathodoluminescence experiments will be performed in the near future to confirm the proposed model.

The general conclusion from our experiment and the literature review is that the role of oxygen is unclear and more research is needed to gain information about microscopic structure of rare earth centers with oxygen.

ACKNOWLEDGMENTS

This work was supported by AFOSR grant No. F49620-1-0024, Ohio University CMSS Program, and Ohio University S.E.E.C.S. Stocker Fund.

REFERENCES

1. H. Ennen and J. Schneider, *J. Electron Mater.*, 13, 115, (1984).
2. V.F. Masterov and L.F. Zakharenkov, *Sov. Phys. Semicond.* 24, 383, (1990).
3. H. Przybylinska, G. Hendorfer, M. Bruckner, L. Palmetshofer, and W. Jantsch, *Appl. Phys. Lett.* 61, 2181, (1994), and references therein.
4. D.L. Adler, D.C. Jacobson, D.J. Eaglesham, M.A. Marcus, J.L. Benton, J.M. Poate, and P. H. Citrin, *Appl. Phys. Lett.* 61, 2181, (1992).
5. M. Needels, M. Schluter and M. Lannoo, *Phys. Rev. B* 457, 15533, (1993).
6. a) F. Auzel, A.M. Jean-Louis, T. Toudic, *J. Appl. Phys.* 66, 3952, (1989), b) P. Galtier, T. Benyattou, J.P. Pocholle, M.N. Charasse, G. Guillot and F.P. Hirz, *Inst. Phys. Conf. Ser.* 106, 327, (1990), c) P.N. Favenne, H. L'Haridon, D. Moutonnet, M. Salvi, M. Gauneau and A. C. Papadopoulos, *Inst. Phys. Conf. Ser.* 106, 333, (1990), d) P.N. Favenne, M. Gauneau, H.L'Haridon, B. Deveaud, C.A. Evans, and R.J. Blattner, *Appl. Phys. Lett.* 38, 271, (1981), e) A.E. Von Neida, S.J. Pearton, W.S. Hobson and C.R. Abernathy, *Appl. Phys. Lett.* 54, 1540, (1989).
7. J.E. Colon, D.W. Elsaesser, Y.K. Yeo, R.L. Hengehold and G.S. Pomrenke, *Appl. Phys. Lett.* 63, 216, (1993).
8. K. Takahei, A. Taguchi, and Y. Horikoshi, *J. Appl. Phys.*, 76, 4332, (1994).
9. a) H. Nakagome, K. Takahei, and Y. Homma, *J. Cryst. Growth*, 85, 345, (1987), b) Aszodi, J. Weber, Ch. Uihlein, L. Pu-lin, H. Ennen, U. Kaufmann, J. Schneider and J. Windscheif, *Phys. Rev. B*, 31, 7767 (1985), c) V.F. Masterov, V.V. Romanov, and K.F. Shtel'mkh, *Sov. Phys. Solid State* 25, 824, (1983)
10. H.J. Lozykowski, A.K. Alshawa and I. Brown, *J. Appl. Phys.* 76, 4836, (1994), and references therein.
11. a) V.A. Kasatkin, F.P. Kesamanly, V.G. Makarenko, and N.S. Tselishcheva, *Sov. Phys. Semicond.* 15, 1414, (1982). b) V.F. Masterov and L.F. Zakharenkov, *Sov. Phys. Semicond.* 24, 383, (1990).
12. H.J. Lozykowski, *Phys. Rev. B* 48, 17758, (1993).
13. a) L. He and W.A. Anderson, *Proceedings of Fourth Int. Conf. on InP and related Materials*, IEEE Catalog # 92CH3104-7, (New York NY, IEEE 1992), p. 336 and references therein. b) P.J. Dean and C.H. Henry, *Phys. Rev.* 176, 928, (1968).
14. H.J. Lozykowski, et al. (in preparation).

3. Tiesheng Li, H. J. Lozykowski, and J. L. Reno,

**“Photoluminescence and Photo-Current Study of a
CdTe / CdZnTe Strained Layer Coupled.”**

Semiconductor Heteroepitaxy

*Growth, Characterization
and Device Applications*

editors

Bernard Gil

Centre National de la Recherche Scientifique, France

Roger-Louis Aulombard

Université de Montpellier II, France



World Scientific

Singapore • New Jersey • London • Hong Kong

PHOTOLUMINESCENCE AND PHOTO-CURRENT STUDY OF A CdTe/CdZnTe STRAINED-LAYER COUPLED DOUBLE QUANTUM WELL STRUCTURE

Tiesheng Li, H. J. Lozykowski, Department of Electrical and Computer Engineering, Ohio University, Athens, OH 45701, and J. Reno, Sandia National Laboratories, Albuquerque, NM 87185-5800

ABSTRACT

Experimental and theoretical investigations of electronic states in a strained-layer CdTe/CdZnTe coupled double quantum well structure are presented. The optical properties of this lattice-mismatched heterostructure were characterized by photoluminescence (PL), photocurrent (PC), PL excitation and polarization spectroscopies. The confined electronic states were calculated in the framework of the envelope function approach, taking into account the strain effect induced by the lattice-mismatch. Experimental results are compared with the calculated transition energies.

INTRODUCTION

In this paper we investigate the photoluminescence, photoluminescence excitation, polarization and photocurrent spectra in $\text{Cd}_{1-x}\text{Zn}_x\text{Te}/\text{CdTe}$ symmetric coupled double quantum wells (CDQW) for the first time, to the best of our knowledge, in II-VI compounds. In symmetric, coupled double quantum wells (CDQW) the electron and hole subband levels are split into levels associated with symmetric and antisymmetric combinations of an isolated single quantum well (SQW) wave functions. The binding of an electron and a heavy-hole in their symmetric states produces a symmetric heavy-hole free-exciton (S-hhFE). Similarly, an antisymmetric heavy-hole free exciton (A-hhFE) is formed from an "antisymmetric" electron and an "antisymmetric" heavy-hole. Our previous study on $\text{CdTe}/\text{Cd}_{1-x}\text{Zn}_x\text{Te}$ SQW's has shown that in this heterostructure system the band lineup is type I for heavy-holes and type II for light-holes¹. Excitonic transitions associated with heavy-holes are observed in PL and correspond to collapse of S-hhFE and A-hhFE. In PLE, with the detection locked on S-hhFE and A-hhFE in the wells, FE in the barrier layer is observed. The circular polarized excitation spectra have confirmed that all observed transitions are associated with heavy-holes. The confined states are calculated in the framework of the three-band envelope function method, taking into account the strain effect due to the lattice mismatch between the barrier and well layers. The binding energies of S-hhFE and A-hhFE are deduced from these calculations and experimental results.

EXPERIMENTAL

The samples studied were nominally symmetric, coupled, $\text{CdTe}/\text{Cd}_{1-x}\text{Zn}_x\text{Te}$ double quantum well structures grown by molecular-beam epitaxy (MBE) on n^+ -type (100) GaAs substrates. To ensure that the (100) orientation was obtained for the layers and to eliminate any possible confusion, we deposited approximately 30Å of

ZnTe to initiate the (100) orientation². After the initial 30Å of ZnTe was deposited, a $\text{Cd}_{1-x}\text{Zn}_x\text{Te}$ layer was grown ($x \sim 0.14$). The mismatch between $\text{Cd}_{0.86}\text{Zn}_{0.14}\text{Te}$ and GaAs is quite large ($\sim 13\%$). This leads to a very high dislocation density in the films. We have found, using both photoluminescence microscopy and X-ray diffraction, that the quality of the CdTe film increases with the thickness until the film is 3 to 4 μm thick^{2c}. There may be some continued improvement in the film beyond this thickness but the improvement is small and it is difficult to verify. Therefore, the underlying CdZnTe buffer layers were grown to a thickness of 4 μm . The coupled quantum wells consisted of two CdTe quantum wells each with a thickness of 75 Å and a CdZnTe barrier. The thicknesses of the barriers were 13, 25, 50, and 75 Å. On top of the coupled quantum wells, a 0.5 μm cap layer of CdZnTe was grown. The buffer layer and CDQW structure are nominally not doped. From the analysis of the X-ray data, the buffer and cap layers were relaxed.

The PL measurements were performed with an Ar^+ laser for the $\text{Cd}_{1-x}\text{Zn}_x\text{Te}$ barriers excitation or by a tunable Ti:Sapphire laser for barrier excitation or directly the CdTe quantum well excitation. The circular polarization of luminescence and excitation spectra was measured using a highly sensitive and absolute apparatus involving a photoelastic modulator³. For PC and PL (under influence of electric field) measurements, a field perpendicular to the interfaces was applied via a semitransparent Schottky contact Au film (10 nm thick) on the top of the cladding $\text{Cd}_x\text{Zn}_{1-x}\text{Te}$ layer. The structure is shown in inset of Fig.1. The build-in electric field was estimated from the flat band condition which occur at voltage 1.0 - 1.13 V. The estimates are based on: (a) an open-circuit photovoltage measured when it saturates for high excitation intensity (above the $\text{Cd}_x\text{Zn}_{1-x}\text{Te}$ band gap), (b) a direction of photocurrent under constant excitation as the function of applied voltage, (determined as the voltage for which the PC crosses the zero value). The PCS measurements involve electric fields that create Stark shifts, and changes in transition strength, and transition life time⁴.

RESULTS AND DISCUSSION

Detailed results are only presented for the sample R813 ($x=1.42$, $L_b=75\text{Å}$) since the results were found similar for each CDQW investigated. Fig. 1a shows the PL spectra of R813 and R835, which is a $\text{Cd}_{1-x}\text{Zn}_x\text{Te}$ epitaxial layer grown on n^+ -type (100) GaAs substrates under conditions similar to the growth of R813. The spectra were taken at $T=9.0\text{ K}$, excited by the 488nm line of Ar^+ laser. By comparison of these spectra, it is clear that only the peak A (at 1.5879eV), and peak B (at 1.6068eV) is from the CDQW structure. After curve fitting and removing the emission peaks from a barrier layer, the "net" emission spectrum of the CDQW is plotted in Fig. 1b. Our previous study on CdTe/ $\text{Cd}_{1-x}\text{Zn}_x\text{Te}$ SQW's¹ has shown that the binding energy of heavy-hole-free-exciton in a 75Å SQW is about 36.5meV. Using this value, peaks, A and B fall into the region for S-hhFE and A-hhFE collapse respectively. The PLE spectrum of peak A is showed in Fig.2. The PLE (dashed line) spectrum is taken with detection locked on the energy of 1.58543 eV, which detects emission from peak A in PL spectrum. The peak at 1.6105eV in the

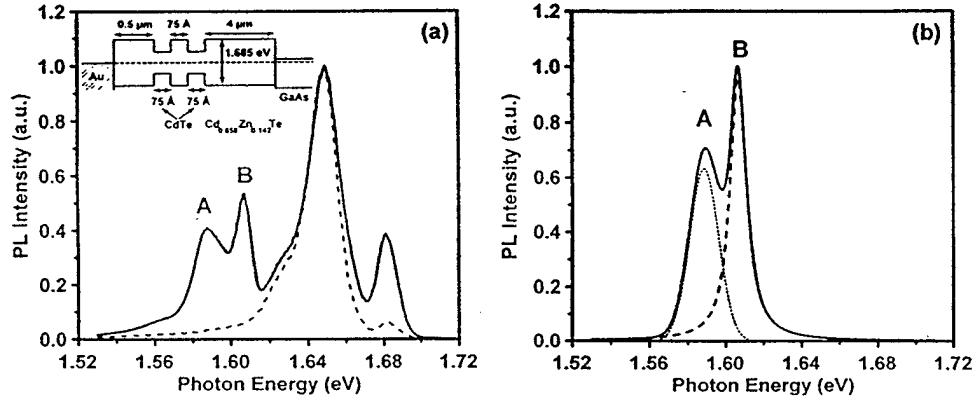


Fig. 1. a. PL spectra from sample R813 and R835, which is a $\text{Cd}_{1-x}\text{Zn}_x\text{Te}$ epitaxy layer grown on n^+ -type (100) GaAs substrates under the condition similar to the growth of R813. The inset is a schematic of the band lineup. b. The "net" emission spectrum of the CDQW and its curve fitting.

Table 2. Calculated and experimental transitions and their difference E_B for all samples studied. The x value is the mole concentration of Zinc in the Barrier layer.

Sample		Transition Type	Calculated Subband Gap (eV)	Experimental Emission Peak Energy (eV)	Exciton Binding Energy (meV)
R810	$x=0.134$	S-hhFE	1.61688	1.58281	34.07
	$L_b=13 \text{ \AA}$	A-hhFE	1.6003	1.56704	33.26
R811	$x=0.143$	S-hhFE	1.6198	1.58308	36.72
	$L_b=25 \text{ \AA}$	A-hhFE	1.63183	1.60601	25.82
R812	$x=0.133$	S-hhFE	1.62217	1.58638	35.79
	$L_b=50 \text{ \AA}$	A-hhFE	1.628	1.60674	21.26
R813	$x=0.142$	S-hhFE	1.62382	1.58876	35.06
	$L_b=75 \text{ \AA}$	A-hhFE	1.62665	1.60691	19.74

PLE spectrum shows that the peaks A and B in PL spectrum are well coupled to each other. The peak at 1.6842 eV in the PLE spectrum is due to the FE formation in the barrier layer. The PLE of peak B is also plotted (solid line) in Fig. 2, which shows a strong peak at the barrier FE energy. Note from Fig. 2 that both peaks A, and B in PL spectrum are strongly coupled to the barrier FE and peaks A, and B are well coupled to each other. The circularly polarized PLE of peak A in PL spectrum is shown in Fig. 3, which clearly shows that both peak A, and peak B in PL spectrum have heavy-hole polarity.

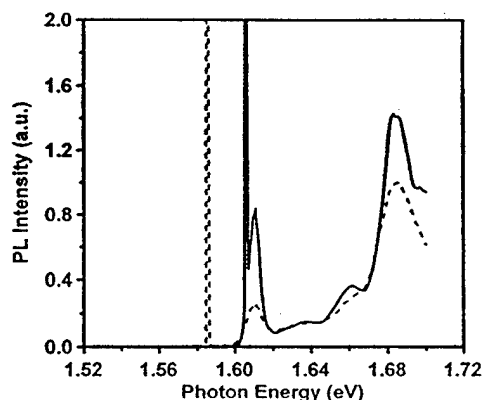


Fig. 2. PL excitation spectra of R813. Dashed line using peak A and solid line using peak B in PL.

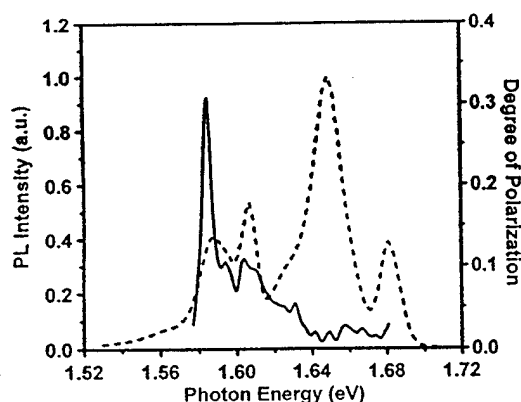


Fig. 3. Circular polarization spectrum of R813.

The calculation shows that in all of four samples studied, there is only one confined level for electrons in the SQW and it is split into two levels, one symmetric and the other antisymmetric. The two heavy-hole levels in the SQW are similarly split into four sublevels, two symmetric and the other two antisymmetric. Light-holes are not confined in CdTe layer due to the strain effect. The only two allowed transitions are between first symmetric electron level (s-e1) and first symmetric heavy-hole level (s-hh1), and first antisymmetric electrons level (a-e1) and first antisymmetric heavy-hole level (a-hh1). Subtracting the peak energy of peak A and B in Fig. 1a from calculated (s-e1 - s-hh1) and (a-e1 - a-hh1), the binding energies for S-hhFE and A-hhFE in sample R813 ($x=1.42$, $L_b=75\text{\AA}$) are deduced to be 35.06 meV and 19.74 meV respectively. Table 2 lists the results of calculations and measurements for all the samples studied. Note in Table 2 that for a given sample, $E_b(\text{S-hhFE}) > E_b(\text{A-hhFE})$, as is expected since S-hhFEs are more confined than A-hhFEs: Heavy-holes and electrons associated with symmetric combination of SQW wave functions lie lower in energy than heavy-holes and electrons associated with antisymmetric combination of SQW wave functions.

The photocurrent spectra for sample R813, plotted versus energy in Fig. 4 for different applied voltage exhibit emerging (splitting) peaks with increasing applied voltage. The arrows show transition energies at zero field for the S-hhFE and A-hhFE excitons respectively. The comparison of PC spectra and the photoluminescence spectra revealed a significant exciton peak shift toward the lower energy. The PL spectrum of R813 at 9.0K with 14.0V bias (field $\sim 3 \times 10^4 \text{ V/cm}$) is compared with the one without bias in Fig. 5. To avoid heating problem and possible wavelength offset between the two, the spectra in Fig. 5 were taken with pulsed bias and a gated photon counter in the same run of wavelength scanning. Fig. 5 shows that, with the applied field, both S-hhFE and A-hhFE peaks became weaker in intensity but S-hhFE shifts ($\sim 2.3 \text{ meV}$) toward lower energy while A-hhFE shifts toward higher energy. This is consistent with theoretical analysis of

Quantum Confined Stark Effect (QCSE) in coupled double quantum wells⁵. Under the perturbation of the applied field, the electrons and the holes associated with S-hhFE and A-hhFE tend to localize in different wells, reducing their oscillator strength and hence reducing PL intensity. Theoretical calculation⁶ has also pointed out that when a moderate electrical field is applied to a CDQW, all of the electronic levels do not behave in a similar fashion. The symmetric levels decrease in energy while antisymmetric levels increase in energy. The details analyses of PC spectra in comparison with PLE and PL spectra will be discussed in separate publication.

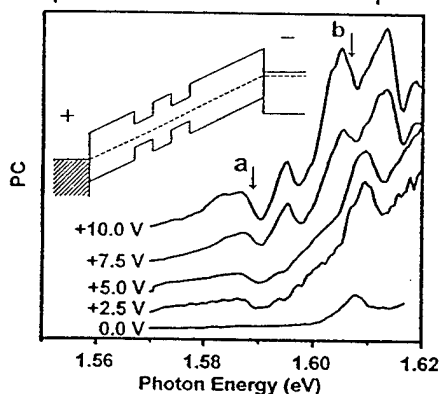


Fig. 4. PC spectra of R813 under positive biases. The inset shows the band structure under bias.

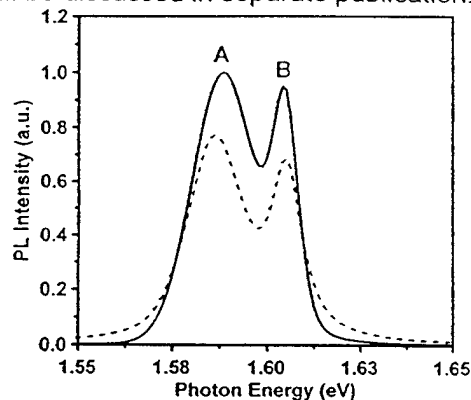


Fig. 5. PL spectra of R813 on and off the 14.0 V bias pulses.

This work was supported by AFOSR grant No. F49620-1-0024, Ohio University CMSS Program, and Ohio University E.C.E. Stocker Fund. Tiesheng Li is supported by the University Post-Doctoral Fellowships program of Ohio University.

REFERENCES :

1. T. Li and H. J. Lozykowski, Phys. Rev. B **46**, 6961, (1992).
2. a. J. L. Reno and E. D. Jones, Phys. Rev. B **45**, 1440 (1992), b. J. P. Faurie, C. Hsu, S. Sivananthan and X. Chu, Surface Science **168**, 473 (1986), c. J. L. Reno, P. L. Gourley, G. Monfroy and J. P. Faurie (unpublished).
3. H. J. Lozykowski, T. Li, and Z. I. Akir, Rev. Sci. Instrum., **V.63**, 4096, (1992).
4. P. W. Yu, G.D. Sanders, D.C. Reynolds, K.K. Bajaj, C.W. Litton, J.Klem, D. Huang, and H. Markoc, Phys. Rev. B **35**, 9250, (1987), and references cited therein.
5. E. S. Koteles, B. Elman, and J. Lee, S. Charbonneau and M. W. L. Thewalt, SPIE Vol. **1283**, *Quantum-Well and Superlattice Physics* (1990), 143
6. G. Bastard, C. Delaland, R. Ferreira, and H.W. Liu, J. Lumin. **44**, (1989), 247